Multiplicity dependence of K*(892)0 and φ(1020) production in pp collisions at √s = 13 TeV

(ALICE Collaboration) Acharya, S.; ...; Antičić, Tome; ...; Erhardt, Filip; ...; Gotovac, Sven; ...; Jerčić, Marko; ...; ...

Physics Letters B 807 (2020) 135501

Contents lists available at ScienceDirect

Physics Letters B

www.elsevier.com/locate/physletb

Multiplicity dependence of $K^*(892)^0$ and $\phi(1020)$ production in pp collisions at $\sqrt{s} = 13$ TeV

ALICE Collaboration *

ARTICLE INFO

Article history:
Received 13 December 2019
Received in revised form 25 March 2020
Accepted 18 May 2020
Available online 28 May 2020
Editor: L. Rolandi

ABSTRACT

The striking similarities that have been observed between high-multiplicity proton-proton (pp) collisions and heavy-ion collisions can be explored through multiplicity-differential measurements of identified hadrons in pp collisions. With these measurements, it is possible to study mechanisms such as collective flow that determine the shapes of hadron transverse momentum (p_T) spectra, to search for possible modifications of the yields of short-lived hadronic resonances due to scattering effects in an extended hadron-gas phase, and to investigate different explanations provided by phenomenological models for enhancement of strangeness production with increasing multiplicity. In this paper, these topics are addressed through measurements of the $K^*(892)^0$ and $\phi(1020)$ mesons at midrapidity in pp collisions at $\sqrt{s} = 13$ TeV as a function of the charged-particle multiplicity. The results include the p_T spectra, p_T-integrated yields, mean transverse momenta, and the ratios of the yields of these resonances to those of longer-lived hadrons. Comparisons with results from other collision systems and energies, as well as predictions from phenomenological models, are also discussed.

1. Introduction

Recent studies of proton-proton (pp) and proton-lead (p–Pb) collisions at the LHC with high charged-particle multiplicities have shown patterns of behavior that are reminiscent of phenomena observed in heavy nucleus-nucleus (A–A) collisions such as Pb–Pb and Xe–Xe. The systems created in these collisions are compared by classifying events according to the final-state charged-particle multiplicity, which is used as a measure of the "activity" of the event. In small collision systems such as pp and p–Pb, multiplicities range from a few to a few tens of charged particles per unit of rapidity, whereas in large systems (A–A collisions), multiplicities of a few thousand charged particles per unit of rapidity can be produced. As discussed below, measurements of azimuthal anisotropies in particle emission [1–7] (quantified using the Fourier coefficients of azimuthal distributions of produced particles), the multiplicity evolution of hadron p_T spectra [8–11], and p_T-differential baryon-to-meson ratios suggest the possibility of collective flow even in small systems. Furthermore, the observed enhancement of strange hadron production [8,9,12] could indicate the production of a quark–gluon plasma (QGP), while the possible suppression of the yields of short-lived resonances [8,11] may suggest the presence of an extended hadronic phase. However, it remains an open question whether the underlying causes of these behaviors are truly the same in small and large collision systems.

In order to investigate this, the ALICE Collaboration has measured the p_T spectra and total yields of identified hadrons as a function of the charged-particle multiplicity in p–Pb collisions at $\sqrt{s_{NN}} = 5.02$ TeV [10,11,13–15] and pp collisions at $\sqrt{s} = 7$ TeV [8,12,16] for many species, including $\pi^{\pm}$, $K^{\pm}$, K^0_S, $K^*(892)^0$, p, $\phi(1020)$, Λ, Ξ^-, Ω^-, deuterons, and their antiparticles. This paper reports on an extension of these studies: a measurement of the multiplicity evolution of the production of $K^*(892)^0$, $\overline{K}^*(892)^0$, and $\phi(1020)$ mesons in pp collisions at $\sqrt{s} = 13$ TeV, the highest energy reached by the LHC in runs 1 and 2. The present study takes advantage of a pp data set recorded during Run 2 of the LHC in 2015 with an integrated luminosity of 0.88 nb^{-1} and complements other recent ALICE papers on light-flavor hadron production in the same collision system, both in inelastic collisions [17] and as a function of charged-particle multiplicity [9,18,19]. For the remainder of this paper, the average of $K^*(892)^0$ and $\overline{K}^*(892)^0$ will be denoted as K^{*0}, while the $\phi(1020)$ will be denoted as ϕ.

The ratios of the yields of strange hadrons to pion yields are observed to be enhanced in A–A collisions relative to minimum bias pp collisions [20–22], with the yields in central A–A collisions being well described by statistical thermal models [23–26]. In central A–A collisions, strangeness is produced from the hadronization of a strangeness-saturated QGP and the relative abundances of hadrons reflect the degree of equilibration of the system. At the LHC, hadron-to-pion yield ratios are observed to increase with the charged-particle multiplicity in pp and p–Pb collisions [8–13]; the magnitude of the change from low to high multiplicity in-

* *E-mail address:* alice-publications@cern.ch.

https://doi.org/10.1016/j.physletb.2020.135501

creases with the strangeness content of the hadron. The ratios in high-multiplicity pp and p–Pb collisions reach the values observed in peripheral Pb–Pb collisions and generally follow similar trends as the multiplicity increases from pp to p–A to A–A collisions. Furthermore, the yields of strange particles are consistent between $\sqrt{s} = 7$ and 13 TeV for similar charged-particle multiplicities. These results suggest that the yields of these hadrons depend primarily on the charged-particle multiplicity and are independent of the collision system and energy. This is perhaps a surprising result: pp, p–Pb, and A–A collisions involve different physical processes (e.g. different contributions from jets and multiple partonic interactions) and produce p_{T} spectra with different shapes. Nevertheless, the total abundances of hadrons, even rare particles like Ω^- and light nuclei, are consistent across the different collision systems for a given charged-particle multiplicity, suggesting that there may be some underlying similarities between the different collision systems. Comparisons of these different collision systems at similar multiplicities may, for example, help to address the question of whether a QGP might be present even in high-multiplicity pp and p–Pb collisions, or alternatively, whether non-QGP effects might explain behavior seen in A–A collisions.

Several theoretical explanations of the multiplicity evolution of strange-hadron production have been put forward, including canonical suppression, rope hadronization, and core-corona effects. In statistical thermal models of large collision systems, strangeness production is described through the use of a grand canonical ensemble, where strangeness conservation is realized on average across the volume of the system. In the canonical suppression picture, strangeness production in small systems is instead described using a canonical ensemble, requiring the exact local conservation of strangeness within the small volume [8,27,28]. As the size of the system decreases, it makes a transition from the grand-canonical to the canonical description, leading to a decrease in strange-hadron yields with decreasing multiplicity. In the rope-hadronization picture, the larger and denser collision systems form color ropes [29–31], groups of overlapping strings that hadronize with a larger effective string tension. This effect, implemented in models such as DIPSY [32–34], also leads to an increase in the production of strange hadrons with increasing charged-particle multiplicity. Core-corona separation is implemented in a variety of models, including EPOS [35–38] and those described in [39,40]. In these models, the collision is divided into "core" and "corona" regions, with the division determined by the string or parton density. Regions with a density greater than the threshold density become the core, which may evolve as a quark–gluon plasma. This is surrounded by a more dilute corona, for which fragmentation occurs as in the vacuum. Strangeness production is higher in the core region, which makes up a greater fraction of the volume of the larger collision systems. This also results in strangeness enhancement with increasing multiplicity.

The ϕ meson is a useful probe for the study of strangeness enhancement. The ϕ contains two strange valence (anti)quarks, but has no net strangeness. Its production should therefore not be canonically suppressed, while the production of hadrons with open strangeness (*e.g.* kaons or Ξ) may be canonically suppressed [8]. It has, in fact, been rather difficult to describe enhancement of ϕ-meson production in a framework that involves canonical suppression [8]. In contrast, in the rope-hadronization or core-corona interpretations, the yields of ϕ mesons evolve with multiplicity similarly to particles with open strangeness, leading to an expected increase in the p_{T}-integrated ϕ/π ratio with increasing charged-particle multiplicity. Measurements of ϕ-meson production as a function of the multiplicity may help to distinguish between the various explanations of strangeness enhancement in small systems.

One of the main motivations for studying resonances like K^{*0} and ϕ in heavy-ion collisions is to learn more about the properties (temperature and lifetime) of the hadronic phase of the collision. When short-lived resonances (such as $\rho(770)^0$, K^{*0}, and $\Lambda(1520)$) decay, their daughters may re-scatter in the hadronic phase, leading to a reduction in the measurable resonance yields; conversely, resonances may also be regenerated due to quasi-elastic scattering of hadrons through a resonance state [41–46]. Centrality-dependent suppression of $\rho(770)^0$, K^{*0}, and $\Lambda(1520)$ production was observed in Pb–Pb collisions [47–50], and a hint of K^{*0} suppression was reported for p–Pb collisions [11]. Observations of a similar suppression in high-multiplicity pp collisions (e.g., the $\mathrm{K}^{*0}/\mathrm{K}$ ratio in pp collisions at $\sqrt{s} = 7$ TeV [8]) might be an indication for a hadronic phase with non-zero lifetime in high-multiplicity pp collisions.

Measurements of identified hadrons can also be used to study collective motion in A–A collisions and to search for similar effects in small collision systems. In non-central A–A collisions, the initial spatial anisotropy in the overlap region of the colliding nuclei results in azimuthally anisotropic pressure gradients in the produced medium, leading to azimuthal anisotropies in particle emission. This anisotropic flow is a manifestation of hydrodynamic behavior in the QGP produced in the A–A collision system. Measurements of azimuthal correlations and anisotropies in particle emission [1–7] also suggest the possibility of collective motion in small collision systems. It was observed that the slopes of hadron p_{T} spectra increase with increasing multiplicity in pp and p–Pb collisions [8–11], while an enhancement in p_{T}-differential baryon-to-meson ratios (e.g. p/π and $\Lambda/\mathrm{K}^0_{\mathrm{S}}$) is observed at intermediate p_{T} ($2 \lesssim p_{\mathrm{T}} \lesssim 7$ GeV/c). This is at least qualitatively similar to the behavior observed in Pb–Pb collisions [51–54], where the effects can be attributed to a collective expansion of the system. In this interpretation, hadrons receive a momentum boost in the direction transverse to the beam axis, which increases in magnitude with increasing multiplicity and is larger for more massive particles. It should be noted, however, that other effects, including recombination [55–57], may be able to account for the observed behavior. The increase in the slopes of the p_{T} spectra is also mirrored in the trend of the measured mean transverse momenta $\langle p_{\mathrm{T}} \rangle$. In contrast to the yields, which evolve along a continuous trend with multiplicity across different collision systems, the $\langle p_{\mathrm{T}} \rangle$ values of light-flavor hadrons follow different trends in pp, p–Pb, and Pb–Pb collisions [10–12,51], with a faster increase for the smaller systems. The $\langle p_{\mathrm{T}} \rangle$ values in the highest multiplicity pp collisions reach, or in some cases exceed, the $\langle p_{\mathrm{T}} \rangle$ values observed in central Pb–Pb collisions. The increase in $\langle p_{\mathrm{T}} \rangle$ in pp collisions is due to changes in the shapes of the p_{T} spectra at low p_{T}; for $p_{\mathrm{T}} \gtrsim 4$ GeV/c, the shapes of hadron p_{T} spectra are essentially independent of multiplicity [9,58]. The color reconnection (CR) mechanism [59–63] describes the interconnections and interactions between strings that originate from different multi-parton interactions. It is implemented in various forms, sometimes including the formation of color ropes, in several event generators based on string fragmentation. Color reconnection can also modify the yields of hadron species (e.g. increasing the rate of baryon formation) and can lead to collective flow-like effects, even in small collision systems and in event generators like PYTHIA that do not include QGP formation.

The results reported here will allow the study of K^{*0} and ϕ production as functions of both energy and multiplicity in pp collisions. The presented results reach higher values of multiplicity than previously measured in pp collisions and therefore provide important additional information on the production of light-flavor hadrons at LHC energies. This paper is organized as follows. The ALICE detector and the criteria adopted for data selection are described in Section 2. A summary of the data analysis procedure is given in Section 3. The results are presented and discussed in Section 4, followed by a summary and conclusions in Section 5.

Table 1
Charged-particle multiplicity densities at midrapidity $\langle dN_{ch}/d\eta \rangle_{|\eta|<0.5}$ for the INEL > 0 class and the various V0M multiplicity classes [9].

Class	$\langle dN_{ch}/d\eta \rangle_{|\eta|<0.5}$
INEL > 0	6.89±0.11
I	25.75±0.40
II	19.83±0.30
III	16.12±0.24
IV	13.76±0.21
V	12.06±0.18
VI	10.11±0.15
VII	8.07±0.12
VIII	6.48±0.10
IX	4.64±0.07
X	2.52±0.04

2. Event and track selection

The ALICE detector is described in detail in [64,65]. The subdetectors that are relevant to the analysis described in this paper are the Time Projection Chamber (TPC), the Time-of-Flight detector (TOF), the Inner Tracking System (ITS), the V0 detectors, and the T0 detectors. The TPC and ITS are used for tracking and finding the primary vertex, while the TPC and TOF are used for particle identification. The V0 detectors (scintillator arrays) and the T0 detectors (arrays of Cherenkov counters) sit on either side of the nominal center of the detector at small angles with respect to the beamline. The V0 detectors are used for triggering and to define the multiplicity estimator at forward rapidities (pseudorapidity ranges $-3.7 < \eta < -1.7$ and $2.8 < \eta < 5.1$). The T0 detectors provide timing information, including a start signal for the TOF.

The K^{*0} and ϕ mesons are reconstructed from a sample of 5×10^7 pp collisions at $\sqrt{s} = 13$ TeV recorded in 2015. The minimum bias trigger required hits in both V0 detectors in coincidence with proton bunches arriving from both directions. Beam-induced background and pile-up events are removed offline; see [9,65] for details. Selected events must also have a primary collision vertex reconstructed with the two innermost layers of the ITS and located within ±10 cm along the beam axis of the nominal center of the ALICE detector. Results in this paper are presented for different event classes corresponding to subdivisions of the "INEL > 0" event class, which is defined as the set of inelastic collisions with at least one charged particle in the range $|\eta| < 1$ [66]. The INEL > 0 sample is divided into multiplicity classes based on the total charge deposited in both V0 detectors (called the "V0M amplitude"). Thus, the event classes are determined by the number of charged particles at forward rapidities, while the K^{*0} and ϕ yields are measured at midrapidity ($|y| < 0.5$); this is to avoid correlations between the K^{*0} and ϕ yields and the multiplicity estimator. Particle yields, yield ratios, and mean transverse momenta are plotted for different multiplicity classes (which correspond to different centralities for A–A collisions) as functions of the corrected mean charged-particle multiplicity density at midrapidity $\langle dN_{ch}/d\eta \rangle_{|\eta|<0.5}$, where η is the pseudorapidity in the lab frame. As in [9], the various multiplicity classes are denoted using Roman numerals, with class I (X) having the highest (lowest) multiplicity. See Table 1 for the values of $\langle dN_{ch}/d\eta \rangle_{|\eta|<0.5}$ measured for each V0M multiplicity class.

Since the K^{*0} and ϕ mesons are short-lived (i.e., their lifetimes are of the order of $\sim 10^{-23}$ s and their decay vertices cannot be distinguished from the primary collision vertex), they cannot be measured directly by the detector. Instead, they are reconstructed via their hadronic decays to charged pions and kaons: $K^{*0} \to \pi^{\pm}K^{\mp}$ (branching ratio $66.503 \pm 0.014\%$) and $\phi \to K^+K^-$ (branching ratio $49.2 \pm 0.5\%$) [67]. Charged tracks are selected using a set of standard track-quality criteria, described in detail in [11]. Pions and kaons are identified using the specific ionization energy loss dE/dx measured in the TPC and the flight time measured in the TOF. Where the dE/dx resolution of the TPC is denoted as σ_{TPC}, pions and kaons are required to have dE/dx values within $2\sigma_{TPC}$ of the expected value for $p > 0.4$ GeV/c, within $4\sigma_{TPC}$ for $0.3 < p < 0.4$ GeV/c, and within $6\sigma_{TPC}$ for $p < 0.3$ GeV/c (typically, $\sigma_{TPC} \sim 5\%$ of the measured dE/dx value). When a pion or kaon track is matched to a hit in the TOF, the time-of-flight value is required to be within $3\sigma_{TOF}$ of the expected value ($\sigma_{TOF} \sim 80$ ps) [68]. These event- and track-selection criteria are varied from their default values and the resulting changes in the yields are incorporated into the systematic uncertainties, which are summarized in Table 2.

3. Data analysis

The K^{*0} and ϕ signals are extracted using the same invariant mass reconstruction method described in [11,17,48]. Invariant mass distributions of unlike-charge πK or KK pairs in the same event are reconstructed after particle identification. The combinatorial background is estimated using multiple methods. In the "like-charge" method, tracks of identical charge from the same event are combined to form pairs. This background is $2\sqrt{n_{--}n_{++}}$, where n_{--} and n_{++} are the number of negative-negative and positive-positive pairs in each invariant mass bin, respectively. In the "mixed-event" method, tracks from one event are combined with oppositely charged tracks from up to 5 other events with similar primary vertex positions and multiplicity percentiles. Specifically, it is required that the longitudinal positions of the primary vertices differ by less than 1 cm and the multiplicity percentiles computed using the V0M amplitude differ by less than 5%. The mixed-event πK (KK) background is normalized so that it has the same integral as the unlike-charge same-event distribution in the invariant mass range $1.1 < m_{\pi K} < 1.15$ GeV/c^2 ($1.05 < m_{KK} < 1.08$ GeV/c^2). In evaluating the systematic uncertainties, the boundaries of the normalization region for the mixed-event background are varied by ~ 100 MeV/c^2 for the K^{*0} analysis and ~ 10 MeV/c^2 for ϕ.

After subtraction of the combinatorial background, the invariant mass distribution consists of a resonance peak sitting on top of a residual background of correlated pairs. This correlated background contains contributions from jets, resonance decays in which a daughter is misidentified, and decays with more than two daughters. In the analysis of the ϕ meson in pp collisions, the signal-to-background ratio is large and the background is observed to vary slowly in the region of the peak. For these reasons, a third approach is also used to describe the background in the ϕ analysis; the combinatorial background is not subtracted, but is instead parameterized together with the residual background using a function as described below. This has the advantage of providing smaller statistical uncertainties than the other methods.

For $p_T < 4$ GeV/c, all three methods provide good descriptions of the KK background and give ϕ yields within a few percent of each other. The final ϕ yields for $p_T < 4$ GeV/c are the averages of those extracted using the three methods of describing the combinatorial background, while the spread among the results for the different methods is incorporated into the systematic uncertainties. As p_T increases, the yields of hadrons decrease, along with the magnitudes of all of the combinatorial backgrounds studied. The mixed-event background, which lacks any contribution from correlated pairs, is observed to become smaller than the same-event (like- or unlike-charge) combinatorial backgrounds as p_T increases, eventually tending to 0 for p_T values higher than the ranges considered here. While the mixed-event background could still be used for the ϕ analysis for $4 \le p_T \le 8$ GeV/c, the two other techniques have smaller statistical fluctuations in this p_T range. Consequently, the mixed-event technique is not used for the analysis

Table 2
Sources of systematic uncertainties for the p_T spectra of K^{*0} and ϕ reported for low, intermediate, and high p_T. When only one value is given for one particle, the uncertainty does not depend on p_T. "Signal extraction" includes variations of the combinatorial background, mixed-event normalization region, fitting region, peak shape, and residual background function. The "signal-loss" uncertainty is multiplicity-dependent, hence values are quoted for the highest and lowest multiplicity classes (I and X, respectively). The text "negl." indicates a negligible uncertainty and "had. int. cross sec." is short for "hadronic interaction cross section."

Particle	K^{*0}			ϕ		
p_T (GeV/c)	0.2	2.2	6.5	0.7	2	6
event/track selection	4.3%	1.6%	2.9%	2.7%	2.9%	3.2%
signal extraction	10.3%	6.7%	7.7%	2.7%	3.1%	3.1%
ITS-TPC matching		2.0%			2.0%	
branching ratio		negl.			1.0%	
material budget	2.0%	0.5%	negl.	5.3%	1.0%	negl.
had. int. cross sec.	2.6%	1.2%	negl.	2.1%	2.6%	negl.
signal loss, class I		negl.			negl.	
signal loss, class X	3.9%	2.4%	0.9%	2.3%	4.8%	2.2%

of ϕ for $p_T > 4$ GeV/c. The mixed-event technique is the primary method used for the extraction of the K^{*0} yields; variations of the yield due to the use of a like-charge background are covered by the systematic uncertainties. However, for $p_T < 0.8$ GeV/c in multiplicity class I, the like-charge method is preferred, since it provides a better description of the background. At high p_T, the mixed-event background for the K^{*0} analysis exhibits the same behavior as for the ϕ, but the problems appear at higher p_T values than for ϕ. The mixed-event technique therefore remains the best available option for this K^{*0} analysis, even at the high end of the p_T range that was studied.

The invariant mass distributions are fitted with a peak function added to a smooth residual background function. For K^{*0}, the peak is described using a Breit-Wigner function. The mass resolution of the detector for the $\phi \to K^-K^+$ channel is of the same order of magnitude as the ϕ width. Therefore, the ϕ peak is described using a Voigt function: a convolution of a Breit-Wigner function and a Gaussian which accounts for the mass resolution of the detector. The K^{*0} and ϕ width parameters are by default fixed to their vacuum values; to calculate the systematic uncertainties, these parameters are allowed to vary freely and the ϕ resolution parameter is fixed to the values (approximately 1–2 MeV/c^2) extracted from the Monte Carlo simulations described below. The residual background is parameterized using a second-order polynomial. To evaluate the systematic uncertainties in the K^{*0} yields, a third-order polynomial is used instead. For the ϕ systematic uncertainties, a first-order polynomial and a function of the form $A + Bm_{KK} + C\sqrt{m_{KK} - 2M(K^{\pm})}$ are used. Here, A, B, and C are free parameters, m_{KK} is the kaon-kaon pair invariant mass, and $M(K^{\pm})$ is the mass of the $K^{\pm}$. The fits are performed in the invariant mass intervals $0.75 < m_{\pi K} < 1.07$ GeV/c^2 for the K^{*0} analysis and $0.995 < m_{KK} < 1.09$ GeV/c^2 for the ϕ. The ranges of the fits are varied by ~ 20 MeV/c^2 for K^{*0} and ~ 10 MeV/c^2 for ϕ; the resulting changes in the yields are included in the systematic uncertainties. Finally, particle yields are extracted by integrating the invariant mass distribution in the peak region ($0.798 \leq m_{\pi K} \leq 0.994$ GeV/c^2 for K^{*0} and $1.01 \leq m_{KK} \leq 1.03$ GeV/c^2 for ϕ), subtracting the integral of the residual background function under the peak, and adding the yields in the tails of the peak fit function outside the integration region. The systematic uncertainty arising from "signal-extraction", as quoted in Table 2, covers the aforementioned variations in the combinatorial background, mixed-event normalization region, residual background function, peak function, and fit range. An additional uncertainty originates from the procedure used to match track segments in the ITS with tracks in the TPC. The branching ratio correction for the ϕ yield introduces a 1% uncertainty, while the corresponding uncertainty for K^{*0} is negligible. Uncertainties in the yields due to uncertainties in the material budget of the detector and the cross sections for hadronic interactions in that material are taken from a previous study [11].

The raw particle yields are corrected for the branching ratios, as well as the acceptance and efficiency of the reconstruction procedure. The correction for acceptance and efficiency (denoted as $A \times \varepsilon$) is calculated using several different event generators (PYTHIA6 Perugia 2011 tune [69], PYTHIA8 Monash 2013 tune [70], and EPOS-LHC [38]), with particles propagated through a simulation of the detector using GEANT3 [71]. No dependence on the generator is observed and the average $A \times \varepsilon$ for the three generators is used in order to reduce statistical fluctuations. This correction is of the same order as reported in [11]. A dependence on multiplicity is observed; for $p_T < 3$ GeV/c, $A \times \varepsilon$ increases by $\sim 10\%$ from multiplicity class I to class X. In the calculation of $A \times \varepsilon$, a weighting procedure is used to account for the fact that (1) $A \times \varepsilon$ may vary significantly over the width of a p_T bin in the measured spectrum and (2) the simulated p_T distributions used in the calculation do not necessarily have the same shapes as the measured p_T distributions. In the Monte Carlo simulations, the generated and reconstructed p_T spectra (the denominator and numerator in the $A \times \varepsilon$ calculation, respectively) are constructed in narrow p_T bins and then weighted using a fit of the measured p_T spectra. The simulated p_T spectra after this weighting are used to recalculate $A \times \varepsilon$ in the wider p_T bins used for the measured p_T spectra. This procedure (also used in [8,9,47,48,50] and others) is repeated until the changes in the correction factor become negligible between iterations; no more than three iterations are needed for the process to converge.

A "signal-loss" correction is also applied, which accounts for K^{*0} and ϕ mesons in non-triggered events. This is evaluated using the same simulations as the acceptance and efficiency. To calculate this correction factor, the simulated resonance p_T spectrum before triggering and event selection is divided by the corresponding p_T spectrum after those selections for each multiplicity class. The signal-loss correction typically deviates from unity by $< 1\%$, but can deviate by $\sim 10\%$ at low p_T for the lowest multiplicity class. Different event generators provide different descriptions of the non-triggered component of the various multiplicity classes. Following [9], the PYTHIA6 simulation is used to obtain the central values for this correction, while an uncertainty is evaluated by comparing the central values to those given by PYTHIA8 and EPOS-LHC. Finally, the p_T spectra are normalized by the number of accepted events and corrected as in [9] to account for INEL > 0 events that do not pass the event-selection criteria. This correction, which is calculated using the PYTHIA6 simulation, is most important (24%) for the lowest multiplicity class and is $< 1\%$ for high-multiplicity collisions (classes I-VIII).

4. Results

The p_T spectra for K^{*0} and ϕ in the various multiplicity classes, as well as the ratios of these spectra to the inclusive INEL > 0 spectrum, are shown in Fig. 1. For $p_T \lesssim 4$ GeV/c the increase in the slopes of the p_T spectra from low to high multiplicity is clearly visible. For higher p_T, the spectra in different multiplicity classes all have the same shape, indicating that the processes that change the shape of the p_T spectra in different multiplicity classes are dominant primarily at low p_T. A similar behavior was reported for unidentified charged hadrons, K^0_S, Λ, Ξ, and Ω for the same collision system [9,58].

The p_T-integrated yields dN/dy and mean transverse momenta $\langle p_T \rangle$ are extracted from the p_T spectra in the different multiplicity classes. For each multiplicity class, the ϕ yield is extrapolated to the unmeasured region ($p_T < 0.5$ GeV/c) by fitting a Lévy-Tsallis function [72–74] to the measured p_T spectra. For multiplicity class

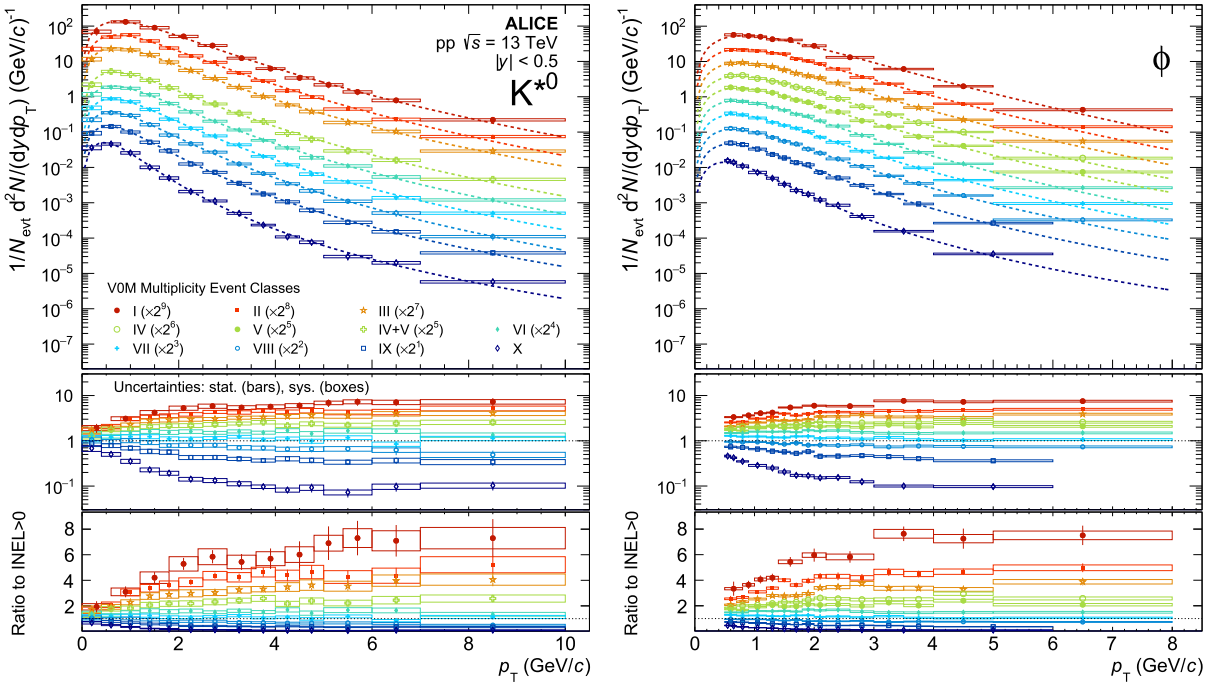

Fig. 1. p_T spectra of K*0 and ϕ in pp collisions at $\sqrt{s} = 13$ TeV for different multiplicity classes, scaled by factors as indicated. The lower panels show the ratios of the multiplicity-dependent p_T spectra to the multiplicity-integrated INEL > 0 spectra (with both linear and logarithmic vertical scales).

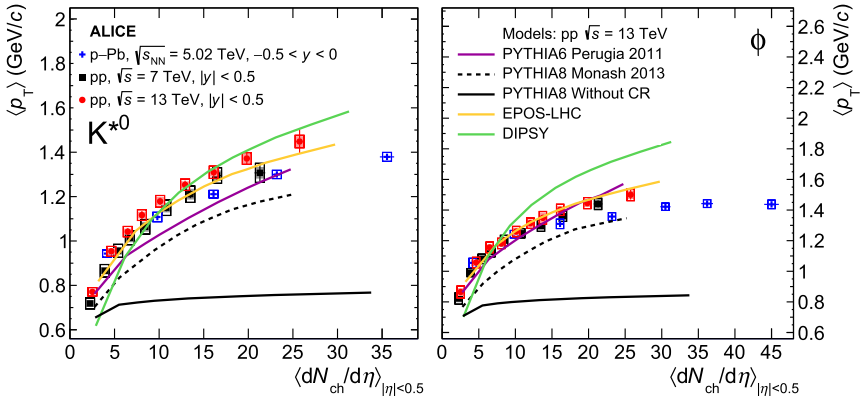

Fig. 2. Mean transverse momenta $\langle p_T \rangle$ of K*0 and ϕ as functions of $\langle dN_{ch}/d\eta \rangle_{|\eta|<0.5}$. Results are shown for pp collisions at $\sqrt{s} = 13$ and 7 TeV [8], as well as for p–Pb collisions at $\sqrt{s_{NN}} = 5.02$ TeV [11]. The measurements in pp collisions at $\sqrt{s} = 13$ TeV are also compared to values from common event generators [33,38,69,70]. Bars represent statistical uncertainties, open boxes represent total systematic uncertainties, and shaded boxes show the systematic uncertainties that are uncorrelated between multiplicity classes (negligible for p–Pb).

I (X) the extrapolated ϕ yield is 12% (34%) of the total yield. The K*0 is measured down to $p_T = 0$ and no low-p_T extrapolation is needed to calculate dN/dy for that particle. The extrapolated yield at high p_T is negligible for both particles. The $\langle p_T \rangle$ is evaluated using the mean value of the fit function within each p_T bin, weighted by the measured yield in each bin. For ϕ, the fit function is used to calculate the yield and mean p_T in the low-p_T extrapolation region, but this is not needed for K*0. The sources of systematic uncertainty for the p_T spectra also contribute to the systematic uncertainties of dN/dy and $\langle p_T \rangle$, except for the ITS-TPC matching and branching ratio uncertainties, which are p_T-independent and do not contribute to the uncertainties of the $\langle p_T \rangle$ values. Additional uncertainties in dN/dy and $\langle p_T \rangle$ of ϕ are evaluated by varying the fit range and the form of the extrapolation function: Bose-Einstein, Boltzmann, and Boltzmann-Gibbs blast-wave [75] distributions, as well as an exponential in m_T (where $m_T \equiv \sqrt{M^2 + p_T^2/c^2}$ and M is the mass of the particle). The uncertainty in the total ϕ yield due to the extrapolation in class I (X) is 1% (4.4%). There is no extrapolation uncertainty for the dN/dy of K*0. Varying the fit function produces a negligible change in $\langle p_T \rangle$ for K*0 and such variations are not included in the systematic uncertainties. The systematic uncertainties on the yield and $\langle p_T \rangle$ are obtained by varying the parameters used in the default analysis. To investigate whether the changes in the yield dN/dy and $\langle p_T \rangle$ are correlated between different multiplicity bins, the effect of changing each parameter is simultaneously evaluated for both the minimum bias event class and each individual multiplicity class. The multiplicity-correlated and uncorrelated components of the systematic uncertainties are separated, with the latter being plotted as shaded boxes in Figs. 2-5.

The mean transverse momenta $\langle p_T \rangle$ for K*0 and ϕ are shown in Fig. 2 as functions of $\langle dN_{ch}/d\eta \rangle_{|\eta|<0.5}$ and compared with other ALICE measurements and results from model calculations. The $\langle p_T \rangle$ values in pp collisions at $\sqrt{s} = 7$ TeV [8] and 13 TeV follow approximately the same trend. The $\langle p_T \rangle$ values of K*0 and ϕ rise slightly faster as a function of $\langle dN_{ch}/d\eta \rangle_{|\eta|<0.5}$ in pp collisions than in p–Pb collisions for $\langle dN_{ch}/d\eta \rangle_{|\eta|<0.5} \gtrsim 5$; the $\langle p_T \rangle$ values in pp and p–Pb collisions both rise faster than those in Pb–Pb

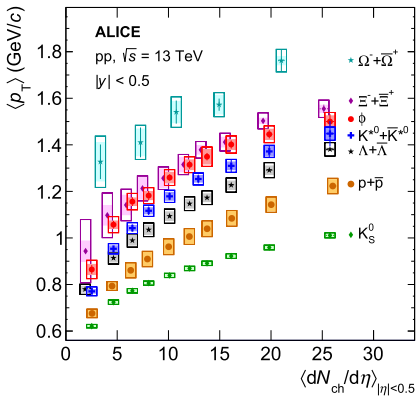

Fig. 3. Mean transverse momenta for K^{*0} and ϕ are compared with those for K^0_S, (anti)protons, $\Lambda+\overline{\Lambda}$, $\Xi^-+\overline{\Xi}^+$, and $\Omega^-+\overline{\Omega}^+$ in pp collisions at $\sqrt{s}=13$ TeV as a function of $\langle dN_{ch}/d\eta \rangle_{|\eta|<0.5}$ [9,18]. The values for $\Lambda+\overline{\Lambda}$ in the lowest multiplicity class and for $\Xi^-+\overline{\Xi}^+$ are shifted horizontally for visibility. Bars represent statistical uncertainties, open boxes represent total systematic uncertainties, and shaded boxes show the systematic uncertainties that are uncorrelated between multiplicity classes.

collisions as discussed in [8,11]. The measured $\langle p_T \rangle$ values are compared with five different model calculations: PYTHIA6 (Perugia 2011 tune) [69], PYTHIA8 (Monash 2013 tune, both with and without color reconnection) [70], EPOS-LHC [38], and DIPSY [33]. PYTHIA8 without color reconnection provides an almost constant $\langle p_T \rangle$ as $\langle dN_{ch}/d\eta \rangle_{|\eta|<0.5}$ increases; this is a very different behavior with respect to the trends measured by ALICE and given by the other model calculations. Turning color reconnection on in PYTHIA8 gives better qualitative agreement with the measurements, although the calculation still somewhat underestimates the $\langle p_T \rangle$ values for hadrons containing strange quarks (K^0_S, K^{*0}, ϕ, Λ, Ξ, and Ω) [9]. Color reconnection in PYTHIA8 introduces a flow-like effect, resulting in an increase in $\langle p_T \rangle$ values with increasing multiplicity without assuming the formation of a medium that could flow [62]. PYTHIA 6 provides a good description of the $\langle p_T \rangle$ values for ϕ, but underestimates $\langle p_T \rangle$ for K^{*0}. The $\langle p_T \rangle$ values predicted by EPOS-LHC are consistent with the measured values for ϕ, but slightly below the values for K^{*0}. Among the model results obtained for the present work, EPOS-LHC gives the best agreement with the measured data. DIPSY gives a larger increase in $\langle p_T \rangle$ from low to high $\langle dN_{ch}/d\eta \rangle_{|\eta|<0.5}$ than is actually observed; this discrepancy is greater for the ϕ and is also observed for other strange hadrons [9].

The values of $\langle p_T \rangle$ for K^{*0} and ϕ are compared with those for K^0_S, (anti)protons, and strange baryons in the same collision system in Fig. 3. In central A–A collisions, a mass ordering of the $\langle p_T \rangle$ values is observed; particles with similar masses (e.g., K^{*0}, p, and ϕ) have similar $\langle p_T \rangle$ [11,51]. This behavior has been interpreted as evidence that radial flow could be a dominant factor in determining the shapes of hadron p_T spectra in central A–A collisions. However, this mass ordering breaks down for peripheral Pb–Pb collisions, as well as p–Pb and pp collisions (see Fig. 7 in [14] and measurements reported in [8,9,18]). In pp collisions at $\sqrt{s}=13$ TeV, the $\langle p_T \rangle$ values for K^{*0} are greater than those for the more massive proton and Λ for the same multiplicity classes. The $\langle p_T \rangle$ values for ϕ exceed those for Λ and even approach those for Ξ, despite the approximately 30% larger mass of the Ξ. This could be a manifestation of differences between the p_T spectra of mesons and baryons or different behavior for resonances in comparison to the longer lived particles. In [8], the Boltzmann-Gibbs blast-wave model was used to predict the p_T spectra of light-flavor hadrons based on a combined fit of $\pi^{\pm}$, $K^{\pm}$, and (anti)proton p_T spectra. This study suggested that strange hadrons (K^0_S, Λ, Ξ, and Ω) and other light-flavor hadrons might participate in a common radial flow, even in pp collisions, but that K^{*0} and ϕ do not follow this common radial expansion (for details of this study, see [8]). The same behavior could result in the violation of mass ordering for $\langle p_T \rangle$ seen at $\sqrt{s}=13$ TeV. A deviation of the $\langle p_T \rangle$ values of short-lived resonances above the trend for other hadrons could in principle be explained by re-scattering of the resonance-decay daughters during the hadronic phase of the collision, which is expected to be most important at low p_T [41]. However, the strongest re-scattering phenomena occur in central A–A collisions, where no deviation from mass ordering is observed. In addition, such effects would be stronger for the shorter lived K^{*0} than for the ϕ, which decays predominantly outside the hadronic phase (even in central A–A collisions) and should be minimally affected by re-scattering. On the other hand, the observed violation of mass ordering could be due to differences between baryon and meson p_T spectra. Baryon-to-meson ratios such as p/π and Λ/K^0_S are observed [8,10] to be enhanced at intermediate p_T (~ 3 GeV/c), even in pp and p–Pb collisions, while similar enhancement is not observed in meson-to-meson ratios like K/π. Differences between baryons and mesons have also been observed in the m_T spectra of hadrons measured at RHIC energies [76,77]. For $m_T \gtrsim 1$ GeV/c, meson m_T spectra follow one common trend, while baryons follow a different, more steeply falling trend as a function of m_T. Such differences between the shapes of baryon and meson spectra may result in mesons having larger $\langle p_T \rangle$ values than baryons with comparable masses. The breakdown of mass ordering, with $\langle p_T(p) \rangle < \langle p_T(K^{*0}) \rangle \approx \langle p_T(\Lambda) \rangle < \langle p_T(\phi) \rangle \approx \langle p_T(\Xi) \rangle$, is a common feature of the models shown in Fig. 2. This behavior may be a consequence of hadron production via fragmentation at high p_T or m_T; meson formation requires only the production of a quark-antiquark pair, while baryon formation requires a diquark-antidiquark pair [76].

The p_T-integrated yields of K^{*0} and ϕ are shown in Fig. 4 as functions of $\langle dN_{ch}/d\eta \rangle_{|\eta|<0.5}$. For both particles, dN/dy exhibits an approximately linear increase with increasing $\langle dN_{ch}/d\eta \rangle_{|\eta|<0.5}$. Results for pp collisions at $\sqrt{s}=7$ and 13 TeV and for p–Pb collisions at $\sqrt{s_{NN}}=5.02$ TeV follow approximately the same trends. This indicates that, for a given multiplicity, K^{*0} and ϕ production rates do not depend on the collision system or energy. Similar results are seen for strange hadrons [9]. The dN/dy values are also compared with those obtained from the same models studied for the discussion of $\langle p_T \rangle$. For the K^{*0}, EPOS-LHC and PYTHIA8 without color reconnection give the best descriptions, the other PYTHIA calculations exhibit fair agreement with the measured data, and DIPSY tends to overestimate the K^{*0} yields. The ϕ yields tend to be slightly overestimated by EPOS-LHC and slightly underestimated by DIPSY, while the PYTHIA calculations underestimate the ϕ yields by about 40%. The selected PYTHIA tunes also underestimate the yields of Λ, Ξ, and Ω by similar factors [9]. For these baryons, the EPOS-LHC description becomes less accurate with increasing strangeness content; DIPSY describes the Λ and Ξ yields well, but underestimates the yields of Ω [9].

The ratios of the p_T-integrated particle yields K^{*0}/K, ϕ/π, ϕ/K, and Ξ/ϕ are shown in Fig. 5 as functions of $\langle dN_{ch}/d\eta \rangle_{|\eta|<0.5}$ [9,18]. Within their uncertainties the ratios in pp collisions at $\sqrt{s}=7$ and 13 TeV and in p–Pb collisions at $\sqrt{s_{NN}}=5.02$ TeV are consistent for similar values of $\langle dN_{ch}/d\eta \rangle_{|\eta|<0.5}$. There is a hint of a decrease in K^{*0}/K with increasing $\langle dN_{ch}/d\eta \rangle_{|\eta|<0.5}$ in all three collision systems; for pp collisions at $\sqrt{s}=13$ TeV the K^{*0}/K ratio in the highest multiplicity class is below the low-multiplicity value at the 2.3σ level (considering only the multiplicity-uncorrelated uncertainties). The decrease in K^{*0}/K in central Pb–Pb collisions [11, 48,49] has been attributed to re-scattering of the K^{*0} decay products in the hadronic phase of the collision [46]. It remains an open question whether a decrease in pp collisions could be caused by the same mechanism. EPOS-LHC provides the best description of the K^{*0}/K ratio in pp collisions at $\sqrt{s}=13$ TeV. PYTHIA and DIPSY

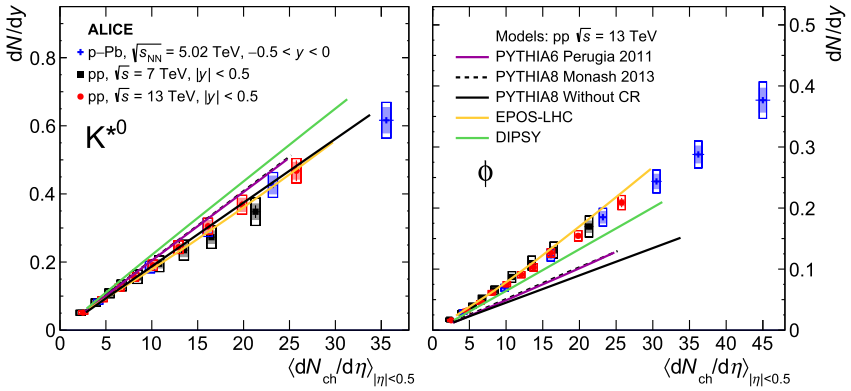

Fig. 4. p_T-integrated yields dN/dy of K^{*0} (average of the particle and antiparticle) and ϕ as functions of $\langle dN_{ch}/d\eta \rangle_{|\eta|<0.5}$. Results are shown for pp collisions at $\sqrt{s} = 13$ and 7 TeV [8], as well as for p–Pb collisions at $\sqrt{s_{NN}} = 5.02$ TeV [11]. The measurements in pp collisions at $\sqrt{s} = 13$ TeV are also compared with values from common event generators [33,38,69,70]. Bars represent statistical uncertainties, open boxes represent total systematic uncertainties, and shaded boxes show the systematic uncertainties that are uncorrelated between multiplicity classes.

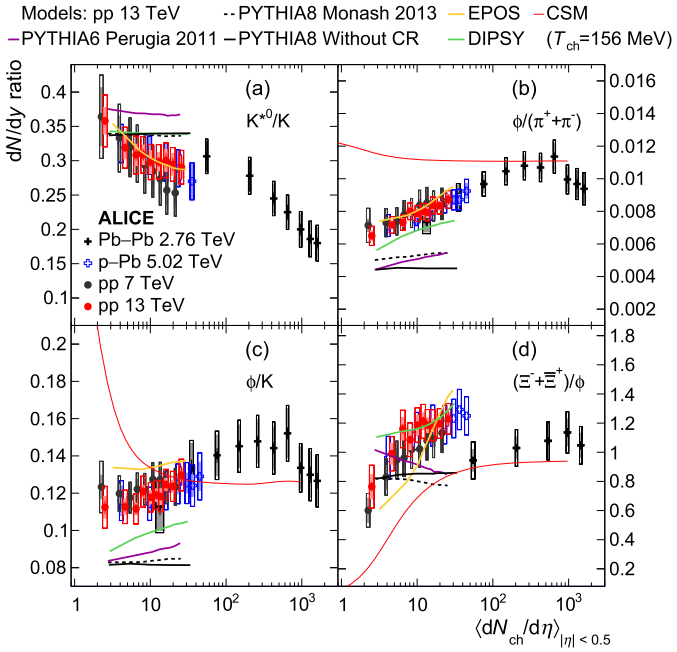

Fig. 5. Ratios of p_T-integrated particle yields K^{*0}/K, ϕ/π, ϕ/K, and Ξ/ϕ in pp collisions at $\sqrt{s} = 13$ TeV as functions of $\langle dN_{ch}/d\eta \rangle_{|\eta|<0.5}$ [9,18]. These measurements are compared with data from pp collisions at $\sqrt{s} = 7$ TeV [8], p–Pb collisions at $\sqrt{s_{NN}} = 5.02$ TeV [11,13], and Pb–Pb collisions at $\sqrt{s_{NN}} = 2.76$ TeV [48,49]. The widths of the boxes for pp collisions at $\sqrt{s} = 13$ TeV and p–Pb collisions do not represent the uncertainties of $\langle dN_{ch}/d\eta \rangle_{|\eta|<0.5}$. The measurements for pp collisions at $\sqrt{s} = 13$ TeV are also compared to results from common event generators [33,38,69,70] and a Canonical Statistical Model calculation [8].

tend to overestimate the ratio for large multiplicities and do not reproduce the apparent decrease with increasing $\langle dN_{ch}/d\eta \rangle_{|\eta|<0.5}$.

The ϕ/π ratio gradually increases from the lowest-multiplicity pp collisions to mid-central Pb–Pb collisions. This ratio compares the yields of two mesons with zero net strangeness, one of which has hidden strangeness. The canonical statistical model (CSM) [8] with a chemical freeze-out temperature of 156 MeV predicts that this ratio should have little dependence on the multiplicity, since the ϕ would not be subject to canonical suppression. The results of the CSM calculation are inconsistent with the observed trend of the ϕ/π ratio. For pp collisions at $\sqrt{s} = 13$ TeV, the increasing trend of the ϕ/π ratio is reproduced fairly well by the EPOS-LHC and DIPSY models, while the PYTHIA calculations underestimate the magnitude of the ratio. The ϕ/K ratio also follows a similar trend in the three collision systems. It is fairly constant as a function of $\langle dN_{ch}/d\eta \rangle_{|\eta|<0.5}$, although there is an apparent small increase with $\langle dN_{ch}/d\eta \rangle_{|\eta|<0.5}$ from the lowest multiplicities up to $\langle dN_{ch}/d\eta \rangle_{|\eta|<0.5} \approx 400$. EPOS-LHC somewhat overestimates the ϕ/K ratio, but is closer to the measured values than PYTHIA, which significantly underestimates ϕ/K. While PYTHIA6 and DIPSY underestimate the ϕ/K ratio, both results exhibit small increases with increasing multiplicity, which is qualitatively similar to the measured trend. The CSM calculation does not describe the behavior of the measured ϕ/K ratio for the $\langle dN_{ch}/d\eta \rangle_{|\eta|<0.5}$ range spanned by the ALICE pp measurements.

In addition to comparing the yields of ϕ to pions and kaons, it may be instructive to compare Ξ and ϕ. These two particles contain the same number of strange valence (anti)quarks: ϕ is a $s\bar{s}$ bound state and Ξ contains two strange valence quarks. However, Ξ would be subject to canonical suppression, unlike the strangeness-neutral ϕ. Fig. 5 also shows the Ξ/ϕ ratio in pp, p–Pb, and Pb–Pb collisions. The ratio increases with increasing $\langle dN_{ch}/d\eta \rangle_{|\eta|<0.5}$ for low-multiplicity collisions and is then fairly constant for a wide range of multiplicities: from pp and p–Pb collisions at $\langle dN_{ch}/d\eta \rangle_{|\eta|<0.5} \approx 7$ to central Pb–Pb collisions. There is a possible small increase in the Ξ/ϕ ratio from $\langle dN_{ch}/d\eta \rangle_{|\eta|<0.5} \approx 7$ to the highest-multiplicity p–Pb collisions, as well as a difference on the 1.5σ level between the p–Pb and Pb–Pb measurements at $\langle dN_{ch}/d\eta \rangle_{|\eta|<0.5} \approx 50$. Nevertheless, there is no clear increase in the ratio for $\langle dN_{ch}/d\eta \rangle_{|\eta|<0.5} \geq 7$. The decrease in Ξ/ϕ with decreasing $\langle dN_{ch}/d\eta \rangle_{|\eta|<0.5}$ for low multiplicities could be interpreted as evidence of canonical suppression in small systems; the canonical statistical model predicts a decrease in the Ξ/ϕ ratio with decreasing $\langle dN_{ch}/d\eta \rangle_{|\eta|<0.5}$ that is qualitatively similar to the measured data. However, canonical suppression would also result in an increase in the ϕ/K ratio with decreasing $\langle dN_{ch}/d\eta \rangle_{|\eta|<0.5}$, which is not observed. Given that Ξ and K have different numbers of strange valence (anti)quarks, it is expected that Ξ would be more affected by canonical suppression [8]. It will be interesting to extend the study of the ϕ/K ratio to lower multiplicities to test if there is any increase in this ratio due to canonical suppression of kaon yields. The measured multiplicity evolution of the Ξ/ϕ and ϕ/K ratios suggests that the ϕ meson behaves as if it had between 1 and 2 units of strangeness: i.e., Ξ is enhanced more than ϕ, which is (possibly) enhanced more than K. In addition, there are indications of increases in the p/π and Λ/K^0_S ratios with increasing $\langle dN_{ch}/d\eta \rangle_{|\eta|<0.5}$ [8,9] which are qualitatively similar to the increase in Ξ/ϕ, but smaller in magnitude. This suggests that baryon-meson differences (e.g., baryon suppression or meson enhancement) might be a contributing factor, but not the only reason, for the low-multiplicity behavior of the Ξ/ϕ ratio. EPOS-LHC, which includes core-corona effects, gives an increasing trend in

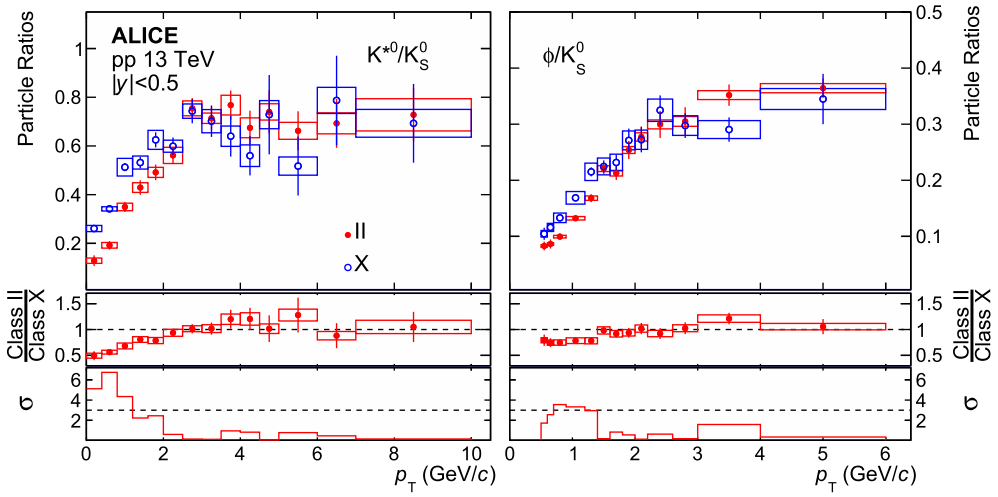

Fig. 6. Ratios of particle yields K^{*0}/K^0_S and ϕ/K^0_S as functions of p_T [9] for low (X) and high (II) multiplicity classes. The middle panels show the double ratios: the measurements in class II divided by those in class X. The significance of the deviations of the double ratios from unity is plotted in the lower panels, with dashed lines indicating a deviation at the 3σ level. Bars represent the statistical uncertainties, while boxes represent the part of the systematic uncertainty that is uncorrelated between multiplicity classes II and X.

Ξ/ϕ with increasing $\langle dN_{ch}/d\eta\rangle_{|\eta|<0.5}$, although the values of the ratio and its flattening at high multiplicity are not particularly well described. In contrast, PYTHIA gives a constant or decreasing value of Ξ/ϕ with increasing $\langle dN_{ch}/d\eta\rangle_{|\eta|<0.5}$, which is inconsistent with the observed trend. DIPSY, which includes rope hadronization, describes the Ξ/ϕ ratio over a wide $\langle dN_{ch}/d\eta\rangle_{|\eta|<0.5}$ range, only failing to describe the decrease in the ratio with decreasing multiplicity for the lowest $\langle dN_{ch}/d\eta\rangle_{|\eta|<0.5}$ values.

The p_T dependence of the particle ratios K^{*0}/K^0_S and ϕ/K^0_S is shown in Fig. 6 for low and high multiplicity classes (X and II, respectively). Both ratios increase at low p_T and saturate for $p_T \gtrsim 2.5$ GeV/c; however, for $p_T \lesssim 2.5$ GeV/c the K^{*0}/K^0_S and ϕ/K^0_S ratios in the high multiplicity class (II) are less than in the lowest multiplicity class (X). This behavior is qualitatively consistent with observations in Pb–Pb collisions at $\sqrt{s_{NN}} = 2.76$ TeV [49], where the K^{*0}/K and ϕ/K ratios at low p_T in central collisions are lower compared to pp collisions. The decrease in the low-p_T K^{*0}/K ratio in central Pb–Pb collisions with respect to pp collisions is larger than the decrease in the ϕ/K ratio, which could be expected due to the presence of re-scattering effects. To quantify the decrease in these particle ratios in pp collisions at $\sqrt{s} = 13$ TeV, the middle panels of Fig. 6 show the double ratios: the high-multiplicity values divided by the low multiplicity values. The double ratios are consistent with unity for $p_T \gtrsim 2.5$ GeV/c, which suggests a common evolution of the p_T spectra for these three mesons. However for $p_T \lesssim 2.5$ GeV/c, the suppression of the K^{*0}/K^0_S ratio from low to high-multiplicity collisions is greater than the suppression of the ϕ/K^0_S ratio. This is quantified in the lower panels of Fig. 6, where the significance of the deviations of the double ratios from unity is shown. For $p_T < 1.2$ GeV/c, the K^{*0}/K^0_S double ratio deviates from unity by 4–6.6 times its standard deviation, while the ϕ/K^0_S double ratio deviates from unity at about the 3σ level for $0.6 < p_T < 1.4$ GeV/c. This difference may be a hint of re-scattering in small collision systems.

5. Conclusions

The ALICE Collaboration has reported measurements of the K^{*0} and ϕ mesons at midrapidity in pp collisions at $\sqrt{s} = 13$ TeV in multiplicity classes. The results have many qualitative similarities to those reported for longer lived hadrons in the same collision system [9,18,19] and are consistent with previous measurements [8] of K^{*0} and ϕ in pp collisions at $\sqrt{s} = 7$ TeV. The slopes of the p_T spectra of K^{*0} and ϕ are observed to increase with increasing multiplicity for $p_T \lesssim 4$ GeV/c, which is qualitatively similar to the collective radial expansion observed in Pb–Pb collisions, but can also be explained through color reconnection. In contrast, the shapes of the p_T spectra are the same for all multiplicity classes at high p_T. Both the p_T-integrated yields and the mean transverse momenta increase with increasing charged-particle multiplicity at midrapidity, with approximately linear increases for the yields. It appears that, for a given multiplicity value, the yields of these particles are independent of collision system and energy, while the $\langle p_T\rangle$ values follow different trends for different collision systems. The mass ordering of the $\langle p_T\rangle$ values observed in central Pb–Pb collisions is violated in pp collisions, with the K^{*0} and ϕ mesons having greater $\langle p_T\rangle$ than baryons with similar masses. The EPOS-LHC model describes the multiplicity dependence of the yields and $\langle p_T\rangle$ fairly well for pp collisions at $\sqrt{s} = 13$ TeV. There are hints that the yields of K^{*0} may be reduced, particularly at low p_T and high multiplicity, by re-scattering of its decay daughters in a short-lived hadron-gas phase in pp collisions; similar behavior is observed in Pb–Pb collisions. The ϕ/π ratio increases with increasing $\langle dN_{ch}/d\eta\rangle_{|\eta|<0.5}$ and the yields of the ϕ meson evolve similarly to particles with 1 and 2 units of open strangeness. The ϕ/K and Ξ/ϕ ratios are both fairly constant, exhibiting only slow increases over wide multiplicity ranges, although the Ξ/ϕ ratio decreases with decreasing $\langle dN_{ch}/d\eta\rangle_{|\eta|<0.5}$ for the lowest multiplicity pp and p–Pb collisions. In high-multiplicity pp and p–Pb collisions, these ratios reach values observed in central Pb–Pb collisions. This multiplicity evolution is not consistent with simple descriptions of canonical suppression, but is qualitatively described by the DIPSY model, which includes rope hadronization effects. These new measurements of the ϕ provide further constraints for theoretical models of strangeness production in small collision systems.

Declaration of competing interest

The authors declare that they have no known competing financial interests or personal relationships that could have appeared to influence the work reported in this paper.

Acknowledgements

The ALICE Collaboration would like to thank all its engineers and technicians for their invaluable contributions to the construction of the experiment and the CERN accelerator teams for the

outstanding performance of the LHC complex. The ALICE Collaboration gratefully acknowledges the resources and support provided by all Grid centres and the Worldwide LHC Computing Grid (WLCG) collaboration. The ALICE Collaboration acknowledges the following funding agencies for their support in building and running the ALICE detector: A. I. Alikhanyan National Science Laboratory (Yerevan Physics Institute) Foundation (ANSL), State Committee of Science and World Federation of Scientists (WFS), Armenia; Austrian Academy of Sciences, Austrian Science Fund (FWF): [M 2467-N36] and Nationalstiftung für Forschung, Technologie und Entwicklung, Austria; Ministry of Communications and High Technologies, National Nuclear Research Center, Azerbaijan; Conselho Nacional de Desenvolvimento Científico e Tecnológico (CNPq), Financiadora de Estudos e Projetos (Finep), Fundação de Amparo à Pesquisa do Estado de São Paulo (FAPESP) and Universidade Federal do Rio Grande do Sul (UFRGS), Brazil; Ministry of Education of China (MOEC), Ministry of Science & Technology of China (MSTC) and National Natural Science Foundation of China (NSFC), China; Ministry of Science and Education and Croatian Science Foundation, Croatia; Centro de Aplicaciones Tecnológicas y Desarrollo Nuclear (CEADEN), Cubaenergía, Cuba; The Ministry of Education, Youth and Sports of the Czech Republic, Czech Republic; The Danish Council for Independent Research Natural Sciences, the Villum Fonden and Danish National Research Foundation (DNRF), Denmark; Helsinki Institute of Physics (HIP), Finland; Commissariat à l'Énergie Atomique (CEA), Institut National de Physique Nucléaire et de Physique des Particules (IN2P3) and Centre National de la Recherche Scientifique (CNRS) and Région des Pays de la Loire, France; Bundesministerium für Bildung und Forschung (BMBF) and GSI Helmholtzzentrum für Schwerionenforschung GmbH, Germany; General Secretariat for Research and Technology, Ministry of Education, Research and Religions, Greece; National Research Development and Innovation Office, Hungary; Department of Atomic Energy, Government of India (DAE), Department of Science and Technology, Government of India (DST), University Grants Commission, Government of India (UGC) and Council of Scientific and Industrial Research (CSIR), India; Indonesian Institute of Science, Indonesia; Centro Fermi - Museo Storico della Fisica e Centro Studi e Ricerche Enrico Fermi and Instituto Nazionale di Fisica Nucleare (INFN), Italy; Institute for Innovative Science and Technology, Nagasaki Institute of Applied Science (IIST), Japanese Ministry of Education, Culture, Sports, Science and Technology (MEXT) and Japan Society for the Promotion of Science (JSPS) KAKENHI, Japan; Consejo Nacional de Ciencia y Tecnología (CONACYT), through Fondo de Cooperación Internacional en Ciencia y Tecnología (FONCICYT) and Dirección General de Asuntos del Personal Academico (DGAPA), Mexico; Nederlandse Organisatie voor Wetenschappelijk Onderzoek (NWO), Netherlands; The Research Council of Norway, Norway; Commission on Science and Technology for Sustainable Development in the South (COMSATS), Pakistan; Pontificia Universidad Católica del Perú, Peru; Ministry of Science and Higher Education and National Science Centre, Poland; Korea Institute of Science and Technology Information and National Research Foundation of Korea (NRF), Republic of Korea; Ministry of Education and Scientific Research, Institute of Atomic Physics and Ministry of Research and Innovation and Institute of Atomic Physics, Romania; Joint Institute for Nuclear Research (JINR), Ministry of Education and Science of the Russian Federation, National Research Centre Kurchatov Institute, Russian Science Foundation and Russian Foundation for Basic Research, Russia; Ministry of Education, Science, Research and Sport of the Slovak Republic, Slovakia; National Research Foundation of South Africa, South Africa; Swedish Research Council (VR) and Knut and Alice Wallenberg Foundation (KAW), Sweden; European Organization for Nuclear Research, Switzerland; Suranaree University of Technology (SUT), National Science and Technology Development Agency (NSDTA) and Office of the Higher Education Commission under NRU project of Thailand, Thailand; Turkish Atomic Energy Agency (TAEK), Turkey; National Academy of Sciences of Ukraine, Ukraine; Science and Technology Facilities Council (STFC), United Kingdom; National Science Foundation of the United States of America (NSF) and United States Department of Energy, Office of Nuclear Physics (DOE NP), United States of America.

References

[1] ALICE Collaboration, B. Abelev, et al., Multi-particle azimuthal correlations in p–Pb and Pb–Pb collisions at the CERN Large Hadron Collider, Phys. Rev. C 90 (2014) 054901, arXiv:1406.2474.

[2] ALICE Collaboration, S. Acharya, et al., Investigations of anisotropic flow using multi-particle azimuthal correlations in pp, p–Pb, Xe–Xe, and Pb–Pb collisions at the LHC, Phys. Rev. Lett. 123 (2019) 142301, arXiv:1903.01790.

[3] CMS Collaboration, V. Khachatryan, et al., Evidence for collectivity in pp collisions at the LHC, Phys. Lett. B 765 (2017) 193–220, arXiv:1606.06198.

[4] ALICE Collaboration, B. Abelev, et al., Long-range angular correlations on the near and away side in p–Pb collisions at $\sqrt{s_{\rm NN}} = 5.02$ TeV, Phys. Lett. B 719 (2013) 29–41, arXiv:1212.2001.

[5] CMS Collaboration, V. Khachatryan, et al., Evidence for collective multi-particle correlations in pPb collisions, Phys. Rev. Lett. 115 (2015) 012301, arXiv:1502.05382.

[6] ATLAS Collaboration, G. Aad, et al., Observation of long-range elliptic anisotropies in $\sqrt{s} = 13$ and 2.76 TeV pp collisions with the ATLAS detector, Phys. Rev. Lett. 116 (2016) 172301, arXiv:1509.04776.

[7] ATLAS Collaboration, M. Aaboud, et al., Measurement of multi-particle azimuthal correlations in pp, p–Pb and low-multiplicity Pb–Pb collisions with the ATLAS detector, Eur. Phys. J. C 77 (2017) 428, arXiv:1705.04176.

[8] ALICE Collaboration, S. Acharya, et al., Multiplicity dependence of light-flavor hadron production in pp collisions at $\sqrt{s} = 7$ TeV, Phys. Rev. C 99 (2019) 024906, arXiv:1807.11321.

[9] ALICE Collaboration, S. Acharya, et al., Multiplicity dependence of (multi-)strange hadron production in proton-proton collisions at $\sqrt{s} = 13$ TeV, Eur. Phys. J. C 80 (2020) 167, arXiv:1908.01861.

[10] ALICE Collaboration, B. Abelev, et al., Multiplicity dependence of pion, kaon, proton and Lambda production in p–Pb collisions at $\sqrt{s_{\rm NN}} = 5.02$ TeV, Phys. Lett. B 728 (2014) 25–38, arXiv:1307.6796.

[11] ALICE Collaboration, J. Adam, et al., Production of $K^*(892)^0$ and $\phi(1020)$ in p–Pb collisions at $\sqrt{s_{\rm NN}} = 5.02$ TeV, Eur. Phys. J. C 76 (2016) 245, arXiv:1601.07868.

[12] ALICE Collaboration, J. Adam, et al., Enhanced production of multi-strange hadrons in high-multiplicity proton-proton collisions, Nat. Phys. 13 (2017) 535–539, arXiv:1606.07424.

[13] ALICE Collaboration, J. Adam, et al., Multi-strange baryon production in p–Pb collisions at $\sqrt{s_{\rm NN}} = 5.02$ TeV, Phys. Lett. B 758 (2016) 389–401, arXiv:1512.07227.

[14] ALICE Collaboration, D. Adamová, et al., Production of $\Sigma(1385)^{\pm}$ and $\Xi(1530)^0$ in p–Pb collisions at $\sqrt{s_{\rm NN}} = 5.02$ TeV, Eur. Phys. J. C 77 (2017) 389, arXiv:1701.07797.

[15] ALICE Collaboration, S. Acharya, et al., Multiplicity dependence of light (anti-)nuclei production in p–Pb collisions at $\sqrt{s_{\rm NN}} = 5.02$ TeV, Phys. Lett. B 800 (2020) 135043, arXiv:1906.03136.

[16] ALICE Collaboration, S. Acharya, et al., Multiplicity dependence of (anti-)deuteron production in pp collisions at $\sqrt{s} = 7$ TeV, Phys. Lett. B 794 (2019) 50–63, arXiv:1902.09290.

[17] ALICE Collaboration, S. Acharya, et al., Production of light-flavor hadrons in pp collisions at $\sqrt{s} = 7$ and $\sqrt{s} = 13$ TeV, arXiv:2005.11120 [nucl-ex].

[18] ALICE Collaboration, S. Acharya, et al., Multiplicity dependence of π, K, and p production in pp collisions at $\sqrt{s} = 13$ TeV, arXiv:2003.02394.

[19] ALICE Collaboration, S. Acharya, et al., (Anti-)deuteron production in pp collisions at $\sqrt{s} = 13$ TeV, arXiv:2003.03184.

[20] NA57 Collaboration, F. Antinori, et al., Enhancement of hyperon production at central rapidity in 158 A GeV/c Pb–Pb collisions, J. Phys. G 32 (2006) 427–442, arXiv:nucl-ex/0601021.

[21] STAR Collaboration, B.I. Abelev, et al., Enhanced strange baryon production in Au+Au collisions compared to $p+p$ at $\sqrt{s_{\rm NN}} = 200$ GeV, Phys. Rev. C 77 (2008) 044908, arXiv:0705.2511.

[22] ALICE Collaboration, B. Abelev, et al., Multistrange baryon production at mid-rapidity in Pb–Pb collisions at $\sqrt{s_{\rm NN}} = 2.76$ TeV, Phys. Lett. B 728 (2014) 216–227, arXiv:1307.5543, Phys. Lett. B 734 (2014) 409–410 (Erratum).

[23] J. Cleymans, I. Kraus, H. Oeschler, K. Redlich, S. Wheaton, Statistical model predictions for particle ratios at $\sqrt{s_{\rm NN}} = 5.5$ TeV, Phys. Rev. C 74 (2006) 034903, arXiv:hep-ph/0604237.

[24] A. Andronic, P. Braun-Munzinger, J. Stachel, Hadron production in central nucleus nucleus collisions at chemical freeze-out, Nucl. Phys. A 772 (2006) 167–199, arXiv:nucl-th/0511071.

[25] A. Andronic, P. Braun-Munzinger, K. Redlich, J. Stachel, The thermal model on the verge of the ultimate test: particle production in Pb–Pb collisions at the LHC, J. Phys. G 38 (2011) 124081, arXiv:1106.6321.

[26] A. Andronic, P. Braun-Munzinger, K. Redlich, J. Stachel, Decoding the phase structure of QCD via particle production at high energy, Nature 561 (2018) 321–330, arXiv:1710.09425.

[27] S. Hamieh, K. Redlich, A. Tounsi, Canonical description of strangeness enhancement from p–A to Pb–Pb collisions, Phys. Lett. B 486 (2000) 61–66, arXiv:hep-ph/0006024.

[28] J. Cleymans, A. Foerster, H. Oeschler, K. Redlich, F. Uhlig, On the chemical equilibration of strangeness-exchange reactions in heavy-ion collisions, Phys. Lett. B 603 (2004) 146–151, arXiv:hep-ph/0406108.

[29] T.S. Biro, H.B. Nielsen, J. Knoll, Colour rope model for extreme relativistic heavy ion collisions, Nucl. Phys. B 245 (1984) 449–468.

[30] A. Bialas, W. Czyz, Chromoelectric flux tubes and the transverse-momentum distribution in high-energy nucleus-nucleus collisions, Phys. Rev. D 31 (1985) 198.

[31] N. Armesto, M.A. Braun, E.G. Ferreiro, C. Pajares, Strangeness enhancement and string fusion in nucleus-nucleus collisions, Phys. Lett. B 344 (1995) 301–307.

[32] E. Avsar, G. Gustafson, L. Lönnblad, Small-x dipole evolution beyond the large-n_c limit, J. High Energy Phys. 1 (2007) 11, arXiv:hep-ph/0610157.

[33] C. Flensburg, G. Gustafson, L. Lönnblad, Inclusive and exclusive observables from dipoles in high energy collisions, J. High Energy Phys. 8 (2011) 103, arXiv:1103.4321.

[34] C. Bierlich, G. Gustafson, L. Lönnblad, A. Tarasov, Effects of overlapping strings in pp collisions, J. High Energy Phys. 3 (2015) 148, arXiv:1412.6259.

[35] H.J. Drescher, et al., Parton-based Gribov-Regge theory, Phys. Rep. 350 (2001) 93–289, arXiv:hep-ph/0007198.

[36] K. Werner, et al., Event-by-event simulation of the three-dimensional hydrodynamic evolution from flux tube initial conditions in ultrarelativistic heavy ion collisions, Phys. Rev. C 82 (2010) 044904, arXiv:1004.0805.

[37] K. Werner, B. Guiot, I. Karpenko, T. Pierog, Analysing radial flow features in p–Pb and p-p collisions at several TeV by studying identified particle production in EPOS3, Phys. Rev. C 89 (2014) 064903, arXiv:1312.1233.

[38] T. Pierog, et al., EPOS LHC: test of collective hadronization with LHC data, Phys. Rev. C 92 (2016) 034906, arXiv:1306.0121.

[39] Y. Kanakubo, M. Okai, Y. Tachibana, T. Hirano, Enhancement of strange baryons in high-multiplicity proton-proton and proton-nucleus collisions, Prog. Theor. Exp. Phys. 2018 (2018) 121D01, arXiv:1806.10329.

[40] Y. Akamatsu, et al., Dynamically integrated transport approach for heavy-ion collisions at high baryon density, Phys. Rev. C 98 (2018) 024909, arXiv:1805.09024.

[41] M. Bleicher, H. Stöcker, Dynamics and freeze-out of hadron resonances at RHIC, J. Phys. G 30 (2004) S111–S118, arXiv:hep-ph/0312278.

[42] G. Torrieri, J. Rafelski, Strange hadron resonances as a signature of freeze-out dynamics, Phys. Lett. B 509 (2001) 239–245, arXiv:hep-ph/0103149.

[43] C. Markert, R. Bellwied, I. Vitev, Formation and decay of hadronic resonances in the QGP, Phys. Lett. B 669 (2008) 92–97, arXiv:0807.1509.

[44] S. Vogel, J. Aichelin, M. Bleicher, Resonances as a possible observable of hot and dense nuclear matter, J. Phys. G 37 (2010) 094046, arXiv:1001.3260.

[45] M. Bleicher, J. Aichelin, Strange resonance production: probing chemical and thermal freeze-out in relativistic heavy ion collisions, Phys. Lett. B 530 (2002) 81–87, arXiv:hep-ph/0201123.

[46] A.G. Knospe, et al., Hadronic resonance production and interaction in partonic and hadronic matter in EPOS3 with and without the hadronic afterburner UrQMD, Phys. Rev. C 93 (2016) 014911, arXiv:1509.07895.

[47] ALICE Collaboration, S. Acharya, et al., $\rho(770)$ production in pp and Pb–Pb collisions at $\sqrt{s_{\rm NN}} = 2.76$ TeV, Phys. Rev. C 99 (2019) 064901, arXiv:1805.04365.

[48] ALICE Collaboration, B. Abelev, et al., $K^*(892)^0$ and $\phi(1020)$ production in Pb–Pb collisions at $\sqrt{s_{\rm NN}} = 2.76$ TeV, Phys. Rev. C 91 (2015) 024609, arXiv:1404.0495.

[49] ALICE Collaboration, J. Adam, et al., $K^*(892)^0$ and $\phi(1020)$ production at high transverse momentum in pp and Pb–Pb collisions at $\sqrt{s_{\rm NN}} = 2.76$ TeV, Phys. Rev. C 95 (2017) 064606, arXiv:1702.00555.

[50] ALICE Collaboration, S. Acharya, et al., Suppression of $\Lambda(1520)$ production in central Pb–Pb collisions at $\sqrt{s_{\rm NN}} = 2.76$ TeV, Phys. Rev. C 99 (2018) 024905, arXiv:1805.04361.

[51] ALICE Collaboration, B. Abelev, et al., Centrality dependence of π, K, and p production in Pb–Pb collisions at $\sqrt{s_{\rm NN}} = 2.76$ TeV, Phys. Rev. C 88 (2013) 044910, arXiv:1303.0737.

[52] ALICE Collaboration, B. Abelev, et al., Production of charged pions, kaons and protons at large transverse momenta in pp and Pb–Pb collisions at $\sqrt{s_{\rm NN}} = 2.76$ TeV, Phys. Lett. B 736 (2014) 196–207, arXiv:1401.1250.

[53] ALICE Collaboration, S. Acharya, et al., Production of charged pions, kaons and (anti-)protons in Pb–Pb and inelastic pp collisions at $\sqrt{s_{\rm NN}} = 5.02$ TeV, arXiv:1910.07678.

[54] ALICE Collaboration, B. Abelev, et al., K^0_S and Λ production in Pb–Pb collisions at $\sqrt{s_{\rm NN}} = 2.76$ TeV, Phys. Rev. Lett. 111 (2013) 222301, arXiv:1307.5530.

[55] V. Greco, C.M. Ko, P. Levai, Parton coalescence and anti-proton / pion anomaly at RHIC, Phys. Rev. Lett. 90 (2003) 202302, arXiv:nucl-th/0301093.

[56] R.J. Fries, B. Muller, C. Nonaka, S.A. Bass, Hadronization in heavy ion collisions: recombination and fragmentation of partons, Phys. Rev. Lett. 90 (2003) 202303, arXiv:nucl-th/0301087.

[57] V. Minissale, F. Scardina, V. Greco, Hadrons from coalescence plus fragmentation in AA collisions at energies available at the BNL Relativistic Heavy Ion Collider to the CERN Large Hadron Collider, Phys. Rev. C 92 (2015) 054904, arXiv:1502.06213.

[58] ALICE Collaboration, S. Acharya, et al., Charged-particle production as a function of multiplicity and transverse spherocity in pp collisions at $\sqrt{s} = 5.02$ and 13 TeV, Eur. Phys. J. C 79 (2019) 857, arXiv:1905.07208.

[59] G. Gustafson, U. Pettersson, P.M. Zerwas, Jet final states in WW pair production and colour screening in the QCD vacuum, Phys. Lett. B 209 (1988) 90–94.

[60] G. Gustafson, J. Häkkinen, Colour interference and confinement effects in W-pair production, Z. Phys. C 64 (1994) 659–664.

[61] T. Sjöstrand, S. Mrenna, P. Skands, PYTHIA 6.4 physics and manual, J. High Energy Phys. 1 (2006) 026, arXiv:hep-ph/0603175.

[62] A. Ortiz Velasquez, et al., Color reconnection and flow-like patterns in pp collisions, Phys. Rev. Lett. 111 (2013) 042001, arXiv:1303.6326.

[63] C. Bierlich, J.R. Christiansen, Effects of colour reconnection on hadron flavour observables, Phys. Rev. D 92 (2015) 094010, arXiv:1507.02091.

[64] ALICE Collaboration, K. Aamodt, et al., The ALICE experiment at the CERN LHC, J. Instrum. 3 (2008), No. S08002 i–245.

[65] ALICE Collaboration, B. Abelev, et al., Performance of the ALICE experiment at the CERN LHC, Int. J. Mod. Phys. A 29 (2014) 1430044, arXiv:1402.4476.

[66] ALICE Collaboration, J. Adam, et al., Pseudorapidity and transverse-momentum distributions of charged particles in proton–proton collisions at $\sqrt{s} = 13$ TeV, Phys. Lett. B 753 (2016) 319–329, arXiv:1509.08734.

[67] Particle Data Group Collaboration, M. Tanabashi, et al., Review of particle physics, Phys. Rev. D 98 (2018) 030001.

[68] ALICE Collaboration, J. Adam, et al., Determination of the event collision time with the ALICE detector at the LHC, Eur. Phys. J. Plus 132 (2017) 99, arXiv:1610.03055.

[69] P.Z. Skands, Tuning Monte Carlo generators: the Perugia tunes, Phys. Rev. D 82 (2010) 074018, arXiv:1005.3457.

[70] P.Z. Skands, S. Carrazza, J. Rojo, Tuning PYTHIA 8.1: the Monash 2013 tune, Eur. Phys. J. C 74 (2014) 3024, arXiv:1404.5630.

[71] R. Brun, F. Carminati, S. Giani, GEANT – Detector Description and Simulation Tool, CERN Program Library Long Writeup W5013, CERN, Geneva, 1994.

[72] C. Tsallis, Possible generalization of Boltzmann-Gibbs statistics, J. Stat. Phys. 52 (1988) 479.

[73] G. Wilk, Z. Włodarczyk, Interpretation of the nonextensitivity parameter q in some applications of Tsallis statistics and Lévy distributions, Phys. Rev. Lett. 84 (2000) 2770, arXiv:hep-ph/9908459.

[74] STAR Collaboration, J. Adams, et al., $K(892)^*$ resonance production in Au+Au and $p + p$ collisions at $\sqrt{s_{\rm NN}} = 200$ GeV at RHIC, Phys. Rev. C 71 (2005) 064902, arXiv:nucl-ex/0412019.

[75] E. Schnedermann, J. Sollfrank, U. Heinz, Thermal phenomenology of hadrons from 200A GeV S+S collisions, Phys. Rev. C 48 (1993) 2462–2475, arXiv:nucl-th/9307020.

[76] STAR Collaboration, B.I. Abelev, et al., Measurements of strange particle production in p+p collisions at $\sqrt{s} = 200$ GeV, Phys. Rev. C 75 (2007) 064901, arXiv:nucl-ex/0607033.

[77] PHENIX Collaboration, A. Adare, et al., Measurement of neutral mesons in p+p collisions at $\sqrt{s} = 200$ GeV and scaling properties of hadron production, Phys. Rev. D 83 (2011) 052004, arXiv:1005.3674.

ALICE Collaboration

S. Acharya [141], D. Adamová [94], A. Adler [74], J. Adolfsson [80], M.M. Aggarwal [99], G. Aglieri Rinella [33], M. Agnello [30], N. Agrawal [10,53], Z. Ahammed [141], S. Ahmad [16], S.U. Ahn [76], A. Akindinov [91], M. Al-Turany [106], S.N. Alam [141], D.S.D. Albuquerque [122], D. Aleksandrov [87], B. Alessandro [58], H.M. Alfanda [6], R. Alfaro Molina [71], B. Ali [16], Y. Ali [14], A. Alici [10,26,53], A. Alkin [2], J. Alme [21], T. Alt [68], L. Altenkamper [21], I. Altsybeev [112], M.N. Anaam [6], C. Andrei [47], D. Andreou [33], H.A. Andrews [110],

A. Andronic [144], M. Angeletti [33], V. Anguelov [103], C. Anson [15], T. Antičić [107], F. Antinori [56], P. Antonioli [53], R. Anwar [125], N. Apadula [79], L. Aphecetche [114], H. Appelshäuser [68], S. Arcelli [26], R. Arnaldi [58], M. Arratia [79], I.C. Arsene [20], M. Arslandok [103], A. Augustinus [33], R. Averbeck [106], S. Aziz [61], M.D. Azmi [16], A. Badalà [55], Y.W. Baek [40], S. Bagnasco [58], X. Bai [106], R. Bailhache [68], R. Bala [100], A. Baldisseri [137], M. Ball [42], S. Balouza [104], R. Barbera [27], L. Barioglio [25], G.G. Barnaföldi [145], L.S. Barnby [93], V. Barret [134], P. Bartalini [6], K. Barth [33], E. Bartsch [68], F. Baruffaldi [28], N. Bastid [134], S. Basu [143], G. Batigne [114], B. Batyunya [75], D. Bauri [48], J.L. Bazo Alba [111], I.G. Bearden [88], C. Bedda [63], N.K. Behera [60], I. Belikov [136], A.D.C. Bell Hechavarria [144], F. Bellini [33], R. Bellwied [125], V. Belyaev [92], G. Bencedi [145], S. Beole [25], A. Bercuci [47], Y. Berdnikov [97], D. Berenyi [145], R.A. Bertens [130], D. Berzano [58], M.G. Besoiu [67], L. Betev [33], A. Bhasin [100], I.R. Bhat [100], M.A. Bhat [3], H. Bhatt [48], B. Bhattacharjee [41], A. Bianchi [25], L. Bianchi [25], N. Bianchi [51], J. Bielčík [36], J. Bielčíková [94], A. Bilandzic [104,117], G. Biro [145], R. Biswas [3], S. Biswas [3], J.T. Blair [119], D. Blau [87], C. Blume [68], G. Boca [139], F. Bock [33,95], A. Bogdanov [92], S. Boi [23], L. Boldizsár [145], A. Bolozdynya [92], M. Bombara [37], G. Bonomi [140], H. Borel [137], A. Borissov [92,144], H. Bossi [146], E. Botta [25], L. Bratrud [68], P. Braun-Munzinger [106], M. Bregant [121], M. Broz [36], E.J. Brucken [43], E. Bruna [58], G.E. Bruno [105], M.D. Buckland [127], D. Budnikov [108], H. Buesching [68], S. Bufalino [30], O. Bugnon [114], P. Buhler [113], P. Buncic [33], Z. Buthelezi [72,131], J.B. Butt [14], J.T. Buxton [96], S.A. Bysiak [118], D. Caffarri [89], A. Caliva [106], E. Calvo Villar [111], R.S. Camacho [44], P. Camerini [24], A.A. Capon [113], F. Carnesecchi [10,26], R. Caron [137], J. Castillo Castellanos [137], A.J. Castro [130], E.A.R. Casula [54], F. Catalano [30], C. Ceballos Sanchez [52], P. Chakraborty [48], S. Chandra [141], W. Chang [6], S. Chapeland [33], M. Chartier [127], S. Chattopadhyay [141], S. Chattopadhyay [109], A. Chauvin [23], C. Cheshkov [135], B. Cheynis [135], V. Chibante Barroso [33], D.D. Chinellato [122], S. Cho [60], P. Chochula [33], T. Chowdhury [134], P. Christakoglou [89], C.H. Christensen [88], P. Christiansen [80], T. Chujo [133], C. Cicalo [54], L. Cifarelli [10,26], F. Cindolo [53], J. Cleymans [124], F. Colamaria [52], D. Colella [52], A. Collu [79], M. Colocci [26], M. Concas [58,ii], G. Conesa Balbastre [78], Z. Conesa del Valle [61], G. Contin [24,127], J.G. Contreras [36], T.M. Cormier [95], Y. Corrales Morales [25], P. Cortese [31], M.R. Cosentino [123], F. Costa [33], S. Costanza [139], P. Crochet [134], E. Cuautle [69], P. Cui [6], L. Cunqueiro [95], D. Dabrowski [142], T. Dahms [104,117], A. Dainese [56], F.P.A. Damas [114,137], M.C. Danisch [103], A. Danu [67], D. Das [109], I. Das [109], P. Das [85], P. Das [3], S. Das [3], A. Dash [85], S. Dash [48], S. De [85], A. De Caro [29], G. de Cataldo [52], J. de Cuveland [38], A. De Falco [23], D. De Gruttola [10], N. De Marco [58], S. De Pasquale [29], S. Deb [49], B. Debjani [3], H.F. Degenhardt [121], K.R. Deja [142], A. Deloff [84], S. Delsanto [25,131], D. Devetak [106], P. Dhankher [48], D. Di Bari [32], A. Di Mauro [33], R.A. Diaz [8], T. Dietel [124], P. Dillenseger [68], Y. Ding [6], R. Divià [33], D.U. Dixit [19], Ø. Djuvsland [21], U. Dmitrieva [62], A. Dobrin [33,67], B. Dönigus [68], O. Dordic [20], A.K. Dubey [141], A. Dubla [106], S. Dudi [99], M. Dukhishyam [85], P. Dupieux [134], R.J. Ehlers [146], V.N. Eikeland [21], D. Elia [52], H. Engel [74], E. Epple [146], B. Erazmus [114], F. Erhardt [98], A. Erokhin [112], M.R. Ersdal [21], B. Espagnon [61], G. Eulisse [33], D. Evans [110], S. Evdokimov [90], L. Fabbietti [104,117], M. Faggin [28], J. Faivre [78], F. Fan [6], A. Fantoni [51], M. Fasel [95], P. Fecchio [30], A. Feliciello [58], G. Feofilov [112], A. Fernández Téllez [44], A. Ferrero [137], A. Ferretti [25], A. Festanti [33], V.J.G. Feuillard [103], J. Figiel [118], S. Filchagin [108], D. Finogeev [62], F.M. Fionda [21], G. Fiorenza [52], F. Flor [125], S. Foertsch [72], P. Foka [106], S. Fokin [87], E. Fragiacomo [59], U. Frankenfeld [106], U. Fuchs [33], C. Furget [78], A. Furs [62], M. Fusco Girard [29], J.J. Gaardhøje [88], M. Gagliardi [25], A.M. Gago [111], A. Gal [136], C.D. Galvan [120], P. Ganoti [83], C. Garabatos [106], E. Garcia-Solis [11], K. Garg [27], C. Gargiulo [33], A. Garibli [86], K. Garner [144], P. Gasik [104,117], E.F. Gauger [119], M.B. Gay Ducati [70], M. Germain [114], J. Ghosh [109], P. Ghosh [141], S.K. Ghosh [3], P. Gianotti [51], P. Giubellino [58,106], P. Giubilato [28], P. Glässel [103], D.M. Goméz Coral [71], A. Gomez Ramirez [74], V. Gonzalez [106], P. González-Zamora [44], S. Gorbunov [38], L. Görlich [118], S. Gotovac [34], V. Grabski [71], L.K. Graczykowski [142], K.L. Graham [110], L. Greiner [79], A. Grelli [63], C. Grigoras [33], V. Grigoriev [92], A. Grigoryan [1], S. Grigoryan [75], O.S. Groettvik [21], F. Grosa [30], J.F. Grosse-Oetringhaus [33], R. Grosso [106], R. Guernane [78], M. Guittiere [114], K. Gulbrandsen [88], T. Gunji [132], A. Gupta [100], R. Gupta [100], I.B. Guzman [44], R. Haake [146], M.K. Habib [106], C. Hadjidakis [61], H. Hamagaki [81], G. Hamar [145], M. Hamid [6], R. Hannigan [119], M.R. Haque [63,85], A. Harlenderova [106], J.W. Harris [146], A. Harton [11], J.A. Hasenbichler [33], H. Hassan [95], D. Hatzifotiadou [10,53], P. Hauer [42], S. Hayashi [132], S.T. Heckel [68,104], E. Hellbär [68], H. Helstrup [35], A. Herghelegiu [47], T. Herman [36], E.G. Hernandez [44], G. Herrera Corral [9], F. Herrmann [144], K.F. Hetland [35], T.E. Hilden [43], H. Hillemanns [33], C. Hills [127], B. Hippolyte [136], B. Hohlweger [104], D. Horak [36], A. Hornung [68], S. Hornung [106], R. Hosokawa [15,133], P. Hristov [33], C. Huang [61], C. Hughes [130], P. Huhn [68], T.J. Humanic [96], H. Hushnud [109], L.A. Husova [144],

N. Hussain [41], S.A. Hussain [14], D. Hutter [38], J.P. Iddon [33,127], R. Ilkaev [108], M. Inaba [133], G.M. Innocenti [33], M. Ippolitov [87], A. Isakov [94], M.S. Islam [109], M. Ivanov [106], V. Ivanov [97], V. Izucheev [90], B. Jacak [79], N. Jacazio [53], P.M. Jacobs [79], S. Jadlovska [116], J. Jadlovsky [116], S. Jaelani [63], C. Jahnke [121], M.J. Jakubowska [142], M.A. Janik [142], T. Janson [74], M. Jercic [98], O. Jevons [110], M. Jin [125], F. Jonas [95,144], P.G. Jones [110], J. Jung [68], M. Jung [68], A. Jusko [110], P. Kalinak [64], A. Kalweit [33], V. Kaplin [92], S. Kar [6], A. Karasu Uysal [77], O. Karavichev [62], T. Karavicheva [62], P. Karczmarczyk [33], E. Karpechev [62], A. Kazantsev [87], U. Kebschull [74], R. Keidel [46], M. Keil [33], B. Ketzer [42], Z. Khabanova [89], A.M. Khan [6], S. Khan [16], S.A. Khan [141], A. Khanzadeev [97], Y. Kharlov [90], A. Khatun [16], A. Khuntia [118], B. Kileng [35], B. Kim [60], B. Kim [133], D. Kim [147], D.J. Kim [126], E.J. Kim [73], H. Kim [17,147], J. Kim [147], J.S. Kim [40], J. Kim [103], J. Kim [147], J. Kim [73], M. Kim [103], S. Kim [18], T. Kim [147], T. Kim [147], S. Kirsch [38,68], I. Kisel [38], S. Kiselev [91], A. Kisiel [142], J.L. Klay [5], C. Klein [68], J. Klein [58], S. Klein [79], C. Klein-Bösing [144], M. Kleiner [68], A. Kluge [33], M.L. Knichel [33], A.G. Knospe [125], C. Kobdaj [115], M.K. Köhler [103], T. Kollegger [106], A. Kondratyev [75], N. Kondratyeva [92], E. Kondratyuk [90], J. Konig [68], P.J. Konopka [33], L. Koska [116], O. Kovalenko [84], V. Kovalenko [112], M. Kowalski [118], I. Králik [64], A. Kravčáková [37], L. Kreis [106], M. Krivda [64,110], F. Krizek [94], K. Krizkova Gajdosova [36], M. Krüger [68], E. Kryshen [97], M. Krzewicki [38], A.M. Kubera [96], V. Kučera [60], C. Kuhn [136], P.G. Kuijer [89], L. Kumar [99], S. Kumar [48], S. Kundu [85], P. Kurashvili [84], A. Kurepin [62], A.B. Kurepin [62], A. Kuryakin [108], S. Kushpil [94], J. Kvapil [110], M.J. Kweon [60], J.Y. Kwon [60], Y. Kwon [147], S.L. La Pointe [38], P. La Rocca [27], Y.S. Lai [79], R. Langoy [129], K. Lapidus [33], A. Lardeux [20], P. Larionov [51], E. Laudi [33], R. Lavicka [36], T. Lazareva [112], R. Lea [24], L. Leardini [103], J. Lee [133], S. Lee [147], F. Lehas [89], S. Lehner [113], J. Lehrbach [38], R.C. Lemmon [93], I. León Monzón [120], E.D. Lesser [19], M. Lettrich [33], P. Lévai [145], X. Li [12], X.L. Li [6], J. Lien [129], R. Lietava [110], B. Lim [17], V. Lindenstruth [38], S.W. Lindsay [127], C. Lippmann [106], M.A. Lisa [96], V. Litichevskyi [43], A. Liu [19], S. Liu [96], W.J. Llope [143], I.M. Lofnes [21], V. Loginov [92], C. Loizides [95], P. Loncar [34], X. Lopez [134], E. López Torres [8], J.R. Luhder [144], M. Lunardon [28], G. Luparello [59], Y. Ma [39], A. Maevskaya [62], M. Mager [33], S.M. Mahmood [20], T. Mahmoud [42], A. Maire [136], R.D. Majka [146], M. Malaev [97], Q.W. Malik [20], L. Malinina [75,iii], D. Mal'Kevich [91], P. Malzacher [106], G. Mandaglio [55], V. Manko [87], F. Manso [134], V. Manzari [52], Y. Mao [6], M. Marchisone [135], J. Mareš [66], G.V. Margagliotti [24], A. Margotti [53], J. Margutti [63], A. Marín [106], C. Markert [119], M. Marquard [68], N.A. Martin [103], P. Martinengo [33], J.L. Martinez [125], M.I. Martínez [44], G. Martínez García [114], M. Martinez Pedreira [33], S. Masciocchi [106], M. Masera [25], A. Masoni [54], L. Massacrier [61], E. Masson [114], A. Mastroserio [52,138], A.M. Mathis [104,117], O. Matonoha [80], P.F.T. Matuoka [121], A. Matyja [118], C. Mayer [118], M. Mazzilli [52], M.A. Mazzoni [57], A.F. Mechler [68], F. Meddi [22], Y. Melikyan [62,92], A. Menchaca-Rocha [71], C. Mengke [6], E. Meninno [29,113], M. Meres [13], S. Mhlanga [124], Y. Miake [133], L. Micheletti [25], D.L. Mihaylov [104], K. Mikhaylov [75,91], A. Mischke [63,i], A.N. Mishra [69], D. Miśkowiec [106], A. Modak [3], N. Mohammadi [33], A.P. Mohanty [63], B. Mohanty [85], M. Mohisin Khan [16,iv], C. Mordasini [104], D.A. Moreira De Godoy [144], L.A.P. Moreno [44], I. Morozov [62], A. Morsch [33], T. Mrnjavac [33], V. Muccifora [51], E. Mudnic [34], D. Mühlheim [144], S. Muhuri [141], J.D. Mulligan [79], M.G. Munhoz [121], R.H. Munzer [68], H. Murakami [132], S. Murray [124], L. Musa [33], J. Musinsky [64], C.J. Myers [125], J.W. Myrcha [142], B. Naik [48], R. Nair [84], B.K. Nandi [48], R. Nania [10,53], E. Nappi [52], M.U. Naru [14], A.F. Nassirpour [80], C. Nattrass [130], R. Nayak [48], T.K. Nayak [85], S. Nazarenko [108], A. Neagu [20], R.A. Negrao De Oliveira [68], L. Nellen [69], S.V. Nesbo [35], G. Neskovic [38], D. Nesterov [112], L.T. Neumann [142], B.S. Nielsen [88], S. Nikolaev [87], S. Nikulin [87], V. Nikulin [97], F. Noferini [10,53], P. Nomokonov [75], J. Norman [78,127], N. Novitzky [133], P. Nowakowski [142], A. Nyanin [87], J. Nystrand [21], M. Ogino [81], A. Ohlson [80,103], J. Oleniacz [142], A.C. Oliveira Da Silva [121,130], M.H. Oliver [146], C. Oppedisano [58], R. Orava [43], A. Ortiz Velasquez [69], A. Oskarsson [80], J. Otwinowski [118], K. Oyama [81], Y. Pachmayer [103], V. Pacik [88], D. Pagano [140], G. Paić [69], J. Pan [143], A.K. Pandey [48], S. Panebianco [137], P. Pareek [49,141], J. Park [60], J.E. Parkkila [126], S. Parmar [99], S.P. Pathak [125], R.N. Patra [141], B. Paul [23,58], H. Pei [6], T. Peitzmann [63], X. Peng [6], L.G. Pereira [70], H. Pereira Da Costa [137], D. Peresunko [87], G.M. Perez [8], E. Perez Lezama [68], V. Peskov [68], Y. Pestov [4], V. Petráček [36], M. Petrovici [47], R.P. Pezzi [70], S. Piano [59], M. Pikna [13], P. Pillot [114], L.O.D.L. Pimentel [88], O. Pinazza [33,53], L. Pinsky [125], C. Pinto [27], S. Pisano [10,51], D. Pistone [55], M. Płoskoń [79], M. Planinic [98], F. Pliquett [68], J. Pluta [142], S. Pochybova [145,i], M.G. Poghosyan [95], B. Polichtchouk [90], N. Poljak [98], A. Pop [47], H. Poppenborg [144], S. Porteboeuf-Houssais [134], V. Pozdniakov [75], S.K. Prasad [3], R. Preghenella [53], F. Prino [58], C.A. Pruneau [143], I. Pshenichnov [62], M. Puccio [25,33], J. Putschke [143], R.E. Quishpe [125], S. Ragoni [110], S. Raha [3], S. Rajput [100], J. Rak [126], A. Rakotozafindrabe [137], L. Ramello [31], F. Rami [136], R. Raniwala [101], S. Raniwala [101], S.S. Räsänen [43], R. Rath [49], V. Ratza [42],

I. Ravasenga [30,89], K.F. Read [95,130], K. Redlich [84,v], A. Rehman [21], P. Reichelt [68], F. Reidt [33], X. Ren [6], R. Renfordt [68], Z. Rescakova [37], J.-P. Revol [10], K. Reygers [103], V. Riabov [97], T. Richert [80,88], M. Richter [20], P. Riedler [33], W. Riegler [33], F. Riggi [27], C. Ristea [67], S.P. Rode [49], M. Rodríguez Cahuantzi [44], K. Røed [20], R. Rogalev [90], E. Rogochaya [75], D. Rohr [33], D. Röhrich [21], P.S. Rokita [142], F. Ronchetti [51], E.D. Rosas [69], K. Roslon [142], A. Rossi [28,56], A. Rotondi [139], A. Roy [49], P. Roy [109], O.V. Rueda [80], R. Rui [24], B. Rumyantsev [75], A. Rustamov [86], E. Ryabinkin [87], Y. Ryabov [97], A. Rybicki [118], H. Rytkonen [126], O.A.M. Saarimaki [43], S. Sadhu [141], S. Sadovsky [90], K. Šafařík [36], S.K. Saha [141], B. Sahoo [48], P. Sahoo [48,49], R. Sahoo [49], S. Sahoo [65], P.K. Sahu [65], J. Saini [141], S. Sakai [133], S. Sambyal [100], V. Samsonov [92,97], D. Sarkar [143], N. Sarkar [141], P. Sarma [41], V.M. Sarti [104], M.H.P. Sas [63], E. Scapparone [53], B. Schaefer [95], J. Schambach [119], H.S. Scheid [68], C. Schiaua [47], R. Schicker [103], A. Schmah [103], C. Schmidt [106], H.R. Schmidt [102], M.O. Schmidt [103], M. Schmidt [102], N.V. Schmidt [68,95], A.R. Schmier [130], J. Schukraft [88], Y. Schutz [33,136], K. Schwarz [106], K. Schweda [106], G. Scioli [26], E. Scomparin [58], M. Šefčík [37], J.E. Seger [15], Y. Sekiguchi [132], D. Sekihata [132], I. Selyuzhenkov [92,106], S. Senyukov [136], D. Serebryakov [62], E. Serradilla [71], A. Sevcenco [67], A. Shabanov [62], A. Shabetai [114], R. Shahoyan [33], W. Shaikh [109], A. Shangaraev [90], A. Sharma [99], A. Sharma [100], H. Sharma [118], M. Sharma [100], N. Sharma [99], A.I. Sheikh [141], K. Shigaki [45], M. Shimomura [82], S. Shirinkin [91], Q. Shou [39], Y. Sibiriak [87], S. Siddhanta [54], T. Siemiarczuk [84], D. Silvermyr [80], G. Simatovic [89], G. Simonetti [33,104], R. Singh [85], R. Singh [100], R. Singh [49], V.K. Singh [141], V. Singhal [141], T. Sinha [109], B. Sitar [13], M. Sitta [31], T.B. Skaali [20], M. Slupecki [126], N. Smirnov [146], R.J.M. Snellings [63], T.W. Snellman [43,126], C. Soncco [111], J. Song [60,125], A. Songmoolnak [115], F. Soramel [28], S. Sorensen [130], I. Sputowska [118], J. Stachel [103], I. Stan [67], P. Stankus [95], P.J. Steffanic [130], E. Stenlund [80], D. Stocco [114], M.M. Storetvedt [35], L.D. Stritto [29], A.A.P. Suaide [121], T. Sugitate [45], C. Suire [61], M. Suleymanov [14], M. Suljic [33], R. Sultanov [91], M. Šumbera [94], S. Sumowidagdo [50], S. Swain [65], A. Szabo [13], I. Szarka [13], U. Tabassam [14], G. Taillepied [134], J. Takahashi [122], G.J. Tambave [21], S. Tang [6,134], M. Tarhini [114], M.G. Tarzila [47], A. Tauro [33], G. Tejeda Muñoz [44], A. Telesca [33], C. Terrevoli [125], D. Thakur [49], S. Thakur [141], D. Thomas [119], F. Thoresen [88], R. Tieulent [135], A. Tikhonov [62], A.R. Timmins [125], A. Toia [68], N. Topilskaya [62], M. Toppi [51], F. Torales-Acosta [19], S.R. Torres [9,120], A. Trifiro [55], S. Tripathy [49], T. Tripathy [48], S. Trogolo [28], G. Trombetta [32], L. Tropp [37], V. Trubnikov [2], W.H. Trzaska [126], T.P. Trzcinski [142], B.A. Trzeciak [63], T. Tsuji [132], A. Tumkin [108], R. Turrisi [56], T.S. Tveter [20], K. Ullaland [21], E.N. Umaka [125], A. Uras [135], G.L. Usai [23], A. Utrobicic [98], M. Vala [37], N. Valle [139], S. Vallero [58], N. van der Kolk [63], L.V.R. van Doremalen [63], M. van Leeuwen [63], P. Vande Vyvre [33], D. Varga [145], Z. Varga [145], M. Varga-Kofarago [145], A. Vargas [44], M. Vasileiou [83], A. Vasiliev [87], O. Vázquez Doce [104,117], V. Vechernin [112], A.M. Veen [63], E. Vercellin [25], S. Vergara Limón [44], L. Vermunt [63], R. Vernet [7], R. Vértesi [145], L. Vickovic [34], Z. Vilakazi [131], O. Villalobos Baillie [110], A. Villatoro Tello [44], G. Vino [52], A. Vinogradov [87], T. Virgili [29], V. Vislavicius [88], A. Vodopyanov [75], B. Volkel [33], M.A. Völkl [102], K. Voloshin [91], S.A. Voloshin [143], G. Volpe [32], B. von Haller [33], I. Vorobyev [104], D. Voscek [116], J. Vrláková [37], B. Wagner [21], M. Weber [113], S.G. Weber [144], A. Wegrzynek [33], D.F. Weiser [103], S.C. Wenzel [33], J.P. Wessels [144], J. Wiechula [68], J. Wikne [20], G. Wilk [84], J. Wilkinson [10,53], G.A. Willems [33], E. Willsher [110], B. Windelband [103], M. Winn [137], W.E. Witt [130], Y. Wu [128], R. Xu [6], S. Yalcin [77], K. Yamakawa [45], S. Yang [21], S. Yano [137], Z. Yin [6], H. Yokoyama [63], I.-K. Yoo [17], J.H. Yoon [60], S. Yuan [21], A. Yuncu [103], V. Yurchenko [2], V. Zaccolo [24], A. Zaman [14], C. Zampolli [33], H.J.C. Zanoli [63], N. Zardoshti [33], A. Zarochentsev [112], P. Závada [66], N. Zaviyalov [108], H. Zbroszczyk [142], M. Zhalov [97], S. Zhang [39], X. Zhang [6], Z. Zhang [6], V. Zherebchevskii [112], D. Zhou [6], Y. Zhou [88], Z. Zhou [21], J. Zhu [6,106], Y. Zhu [6], A. Zichichi [10,26], M.B. Zimmermann [33], G. Zinovjev [2], N. Zurlo [140]

[1] *A.I. Alikhanyan National Science Laboratory (Yerevan Physics Institute) Foundation, Yerevan, Armenia*
[2] *Bogolyubov Institute for Theoretical Physics, National Academy of Sciences of Ukraine, Kiev, Ukraine*
[3] *Bose Institute, Department of Physics and Centre for Astroparticle Physics and Space Science (CAPSS), Kolkata, India*
[4] *Budker Institute for Nuclear Physics, Novosibirsk, Russia*
[5] *California Polytechnic State University, San Luis Obispo, CA, United States*
[6] *Central China Normal University, Wuhan, China*
[7] *Centre de Calcul de l'IN2P3, Villeurbanne, Lyon, France*
[8] *Centro de Aplicaciones Tecnológicas y Desarrollo Nuclear (CEADEN), Havana, Cuba*
[9] *Centro de Investigación y de Estudios Avanzados (CINVESTAV), Mexico City and Mérida, Mexico*
[10] *Centro Fermi – Museo Storico della Fisica e Centro Studi e Ricerche "Enrico Fermi', Rome, Italy*
[11] *Chicago State University, Chicago, IL, United States*
[12] *China Institute of Atomic Energy, Beijing, China*
[13] *Comenius University Bratislava, Faculty of Mathematics, Physics and Informatics, Bratislava, Slovakia*
[14] *COMSATS University Islamabad, Islamabad, Pakistan*

[15] Creighton University, Omaha, NE, United States
[16] Department of Physics, Aligarh Muslim University, Aligarh, India
[17] Department of Physics, Pusan National University, Pusan, Republic of Korea
[18] Department of Physics, Sejong University, Seoul, Republic of Korea
[19] Department of Physics, University of California, Berkeley, CA, United States
[20] Department of Physics, University of Oslo, Oslo, Norway
[21] Department of Physics and Technology, University of Bergen, Bergen, Norway
[22] Dipartimento di Fisica dell'Università 'La Sapienza' and Sezione INFN, Rome, Italy
[23] Dipartimento di Fisica dell'Università and Sezione INFN, Cagliari, Italy
[24] Dipartimento di Fisica dell'Università and Sezione INFN, Trieste, Italy
[25] Dipartimento di Fisica dell'Università and Sezione INFN, Turin, Italy
[26] Dipartimento di Fisica e Astronomia dell'Università and Sezione INFN, Bologna, Italy
[27] Dipartimento di Fisica e Astronomia dell'Università and Sezione INFN, Catania, Italy
[28] Dipartimento di Fisica e Astronomia dell'Università and Sezione INFN, Padova, Italy
[29] Dipartimento di Fisica 'E.R. Caianiello' dell'Università and Gruppo Collegato INFN, Salerno, Italy
[30] Dipartimento DISAT del Politecnico and Sezione INFN, Turin, Italy
[31] Dipartimento di Scienze e Innovazione Tecnologica dell'Università del Piemonte Orientale and INFN Sezione di Torino, Alessandria, Italy
[32] Dipartimento Interateneo di Fisica 'M. Merlin' and Sezione INFN, Bari, Italy
[33] European Organization for Nuclear Research (CERN), Geneva, Switzerland
[34] Faculty of Electrical Engineering, Mechanical Engineering and Naval Architecture, University of Split, Split, Croatia
[35] Faculty of Engineering and Science, Western Norway University of Applied Sciences, Bergen, Norway
[36] Faculty of Nuclear Sciences and Physical Engineering, Czech Technical University in Prague, Prague, Czech Republic
[37] Faculty of Science, P.J. Šafárik University, Košice, Slovakia
[38] Frankfurt Institute for Advanced Studies, Johann Wolfgang Goethe-Universität Frankfurt, Frankfurt, Germany
[39] Fudan University, Shanghai, China
[40] Gangneung-Wonju National University, Gangneung, Republic of Korea
[41] Gauhati University, Department of Physics, Guwahati, India
[42] Helmholtz-Institut für Strahlen- und Kernphysik, Rheinische Friedrich-Wilhelms-Universität Bonn, Bonn, Germany
[43] Helsinki Institute of Physics (HIP), Helsinki, Finland
[44] High Energy Physics Group, Universidad Autónoma de Puebla, Puebla, Mexico
[45] Hiroshima University, Hiroshima, Japan
[46] Hochschule Worms, Zentrum für Technologietransfer und Telekommunikation (ZTT), Worms, Germany
[47] Horia Hulubei National Institute of Physics and Nuclear Engineering, Bucharest, Romania
[48] Indian Institute of Technology Bombay (IIT), Mumbai, India
[49] Indian Institute of Technology Indore, Indore, India
[50] Indonesian Institute of Sciences, Jakarta, Indonesia
[51] INFN, Laboratori Nazionali di Frascati, Frascati, Italy
[52] INFN, Sezione di Bari, Bari, Italy
[53] INFN, Sezione di Bologna, Bologna, Italy
[54] INFN, Sezione di Cagliari, Cagliari, Italy
[55] INFN, Sezione di Catania, Catania, Italy
[56] INFN, Sezione di Padova, Padova, Italy
[57] INFN, Sezione di Roma, Rome, Italy
[58] INFN, Sezione di Torino, Turin, Italy
[59] INFN, Sezione di Trieste, Trieste, Italy
[60] Inha University, Incheon, Republic of Korea
[61] Institut de Physique Nucléaire d'Orsay (IPNO), Institut National de Physique Nucléaire et de Physique des Particules (IN2P3/CNRS), Université de Paris-Sud, Université Paris-Saclay, Orsay, France
[62] Institute for Nuclear Research, Academy of Sciences, Moscow, Russia
[63] Institute for Subatomic Physics, Utrecht University/Nikhef, Utrecht, Netherlands
[64] Institute of Experimental Physics, Slovak Academy of Sciences, Košice, Slovakia
[65] Institute of Physics, Homi Bhabha National Institute, Bhubaneswar, India
[66] Institute of Physics of the Czech Academy of Sciences, Prague, Czech Republic
[67] Institute of Space Science (ISS), Bucharest, Romania
[68] Institut für Kernphysik, Johann Wolfgang Goethe-Universität Frankfurt, Frankfurt, Germany
[69] Instituto de Ciencias Nucleares, Universidad Nacional Autónoma de México, Mexico City, Mexico
[70] Instituto de Física, Universidade Federal do Rio Grande do Sul (UFRGS), Porto Alegre, Brazil
[71] Instituto de Física, Universidad Nacional Autónoma de México, Mexico City, Mexico
[72] iThemba LABS, National Research Foundation, Somerset West, South Africa
[73] Jeonbuk National University, Jeonju, Republic of Korea
[74] Johann-Wolfgang-Goethe Universität Frankfurt Institut für Informatik, Fachbereich Informatik und Mathematik, Frankfurt, Germany
[75] Joint Institute for Nuclear Research (JINR), Dubna, Russia
[76] Korea Institute of Science and Technology Information, Daejeon, Republic of Korea
[77] KTO Karatay University, Konya, Turkey
[78] Laboratoire de Physique Subatomique et de Cosmologie, Université Grenoble-Alpes, CNRS-IN2P3, Grenoble, France
[79] Lawrence Berkeley National Laboratory, Berkeley, CA, United States
[80] Lund University Department of Physics, Division of Particle Physics, Lund, Sweden
[81] Nagasaki Institute of Applied Science, Nagasaki, Japan
[82] Nara Women's University (NWU), Nara, Japan
[83] National and Kapodistrian University of Athens, School of Science, Department of Physics, Athens, Greece
[84] National Centre for Nuclear Research, Warsaw, Poland
[85] National Institute of Science Education and Research, Homi Bhabha National Institute, Jatni, India
[86] National Nuclear Research Center, Baku, Azerbaijan
[87] National Research Centre Kurchatov Institute, Moscow, Russia
[88] Niels Bohr Institute, University of Copenhagen, Copenhagen, Denmark
[89] Nikhef, National institute for subatomic physics, Amsterdam, Netherlands
[90] NRC Kurchatov Institute IHEP, Protvino, Russia
[91] NRC «Kurchatov Institute» – ITEP, Moscow, Russia
[92] NRNU Moscow Engineering Physics Institute, Moscow, Russia
[93] Nuclear Physics Group, STFC Daresbury Laboratory, Daresbury, United Kingdom

[94] Nuclear Physics Institute of the Czech Academy of Sciences, Řež u Prahy, Czech Republic
[95] Oak Ridge National Laboratory, Oak Ridge, TN, United States
[96] Ohio State University, Columbus, OH, United States
[97] Petersburg Nuclear Physics Institute, Gatchina, Russia
[98] Physics department, Faculty of science, University of Zagreb, Zagreb, Croatia
[99] Physics Department, Panjab University, Chandigarh, India
[100] Physics Department, University of Jammu, Jammu, India
[101] Physics Department, University of Rajasthan, Jaipur, India
[102] Physikalisches Institut, Eberhard-Karls-Universität Tübingen, Tübingen, Germany
[103] Physikalisches Institut, Ruprecht-Karls-Universität Heidelberg, Heidelberg, Germany
[104] Physik Department, Technische Universität München, Munich, Germany
[105] Politecnico di Bari, Bari, Italy
[106] Research Division and ExtreMe Matter Institute EMMI, GSI Helmholtzzentrum für Schwerionenforschung GmbH, Darmstadt, Germany
[107] Rudjer Bošković Institute, Zagreb, Croatia
[108] Russian Federal Nuclear Center (VNIIEF), Sarov, Russia
[109] Saha Institute of Nuclear Physics, Homi Bhabha National Institute, Kolkata, India
[110] School of Physics and Astronomy, University of Birmingham, Birmingham, United Kingdom
[111] Sección Física, Departamento de Ciencias, Pontificia Universidad Católica del Perú, Lima, Peru
[112] St. Petersburg State University, St. Petersburg, Russia
[113] Stefan Meyer Institut für Subatomare Physik (SMI), Vienna, Austria
[114] SUBATECH, IMT Atlantique, Université de Nantes, CNRS-IN2P3, Nantes, France
[115] Suranaree University of Technology, Nakhon Ratchasima, Thailand
[116] Technical University of Košice, Košice, Slovakia
[117] Technische Universität München, Excellence Cluster 'Universe', Munich, Germany
[118] The Henryk Niewodniczanski Institute of Nuclear Physics, Polish Academy of Sciences, Cracow, Poland
[119] The University of Texas at Austin, Austin, TX, United States
[120] Universidad Autónoma de Sinaloa, Culiacán, Mexico
[121] Universidade de São Paulo (USP), São Paulo, Brazil
[122] Universidade Estadual de Campinas (UNICAMP), Campinas, Brazil
[123] Universidade Federal do ABC, Santo Andre, Brazil
[124] University of Cape Town, Cape Town, South Africa
[125] University of Houston, Houston, TX, United States
[126] University of Jyväskylä, Jyväskylä, Finland
[127] University of Liverpool, Liverpool, United Kingdom
[128] University of Science and Technology of China, Hefei, China
[129] University of South-Eastern Norway, Tonsberg, Norway
[130] University of Tennessee, Knoxville, TN, United States
[131] University of the Witwatersrand, Johannesburg, South Africa
[132] University of Tokyo, Tokyo, Japan
[133] University of Tsukuba, Tsukuba, Japan
[134] Université Clermont Auvergne, CNRS/IN2P3, LPC, Clermont-Ferrand, France
[135] Université de Lyon, Université Lyon 1, CNRS/IN2P3, IPN-Lyon, Villeurbanne, Lyon, France
[136] Université de Strasbourg, CNRS, IPHC UMR 7178, F-67000 Strasbourg, France, Strasbourg, France
[137] Université Paris-Saclay Centre d'Etudes de Saclay (CEA), IRFU, Département de Physique Nucléaire (DPhN), Saclay, France
[138] Università degli Studi di Foggia, Foggia, Italy
[139] Università degli Studi di Pavia, Pavia, Italy
[140] Università di Brescia, Brescia, Italy
[141] Variable Energy Cyclotron Centre, Homi Bhabha National Institute, Kolkata, India
[142] Warsaw University of Technology, Warsaw, Poland
[143] Wayne State University, Detroit, MI, United States
[144] Westfälische Wilhelms-Universität Münster, Institut für Kernphysik, Münster, Germany
[145] Wigner Research Centre for Physics, Budapest, Hungary
[146] Yale University, New Haven, CT, United States
[147] Yonsei University, Seoul, Republic of Korea

[i] Deceased.
[ii] Dipartimento DET del Politecnico di Torino, Turin, Italy.
[iii] M.V. Lomonosov Moscow State University, D.V. Skobeltsyn Institute of Nuclear, Physics, Moscow, Russia.
[iv] Department of Applied Physics, Aligarh Muslim University, Aligarh, India.
[v] Institute of Theoretical Physics, University of Wroclaw, Poland.